RUHR-UNIVERSITÄT BOCHUM

RUB

Surface State Studies near 1-dimensional Defects: Detailed Analysis of Microscopic and Spectroscopic via STM Measurements.

Masterarbeit

im

Studiengang

IMOS

im Fach Chemie

an der Fakultät für Chemie und Biochemie

der Ruhr-Universität Bochum

von

Sinan Nazimuddin Fazal

Bochum, 06.11.2021

Preface

COVID-19 has affected many lives around the world. One of our lab members was stopped due to the closing of the National Borders. This affected our research goals and especially the thesis work. The thesis work and the STM instrumentation require gentle treatment and approach, and guidance is a mandatory ingredient for success. Since the restriction of traveling back was not lifted for one whole year, I have to switch to analyze the work of the former Ph.D. student of Prof. Dr. Karina Morgenstern for my master thesis. The STM measurements used in this thesis were done by Sarah-Charlotta Heidorn and Andre Sabellek in 2009 in the laboratories of the Institute for Solid State Physics at the Leibniz University of Hannover. Whereas all other calculations and analyses are done by myself in the given period of master thesis.

Abstract

In this master thesis project, a detailed analysis of microscopic and spectroscopic STM results is carried out to investigate and to evaluate the electron local density of the states (LDOS) or the surface state of the electron near 1-dimensional defects. The studies include slip plane dislocations and step edge defects on Ag(111) substrate, and NaCl(100) adsorbate induced line-like defects on Ag(111). These defects offer a structural barrier to the electrons, and thus, affect the behavior and dynamics, and open different scattering processes. Moreover, confinement-like phenomena have allowed researching electron LDOS in the presence of these defects. Further, these confinement systems can be categorized into homo-substrate and hetero-substrate topography. Here, the confinement systems exhibited the change in the electronic behavior, raise in the energy eigenstate, and the elimination of the perturbations at higher energies compared to the non-confined 1-dimensional defects. Our evaluation of the work allows us to materialize phenomena and offer promising results toward surface band engineering and confinement from the perspective of a 1-dimensional defect. All the experiments are carried out using Scanning Tunneling Microscopy for local imaging and Spectroscopy mode for evaluating the surface state of the electron.

Contents

1. Introduction

Our work precedes and acknowledges the idea attached to the nanoscopic view of the surface – interaction and transfer of charge across the molecule and substrate, i.e., electron. To understand the 'electron' nature, a couple of methods have been researched and maneuvered. The most well-known ones are Angle-Resolved Photoemission Spectroscopy (ARPES or PES), 2-Photon Photoemission (2PPE), and Scanning Tunneling Microscopy (STM) [1]. An STM is one of the instruments in delivering a single molecule precision and maneuvring them on a nanometre scale [2,3]. Further, an STM has defied the limits of conventional surface analytical techniques [4] and managed to decipher the electronic behavior via its spectroscopy modes [3]. Since the local environment governs the electron behavior, the possible changes facilitate us to understand the characteristics of the system either as a whole or of an individual entity [2].

The motivation for this work lies in exploring the surface state electron behavior and dynamics near the defects. A defect can be a 0-dimensional (Point) and 1-dimensional (Line) defect [5]. This work is entirely based on the surface state of the electron near a 1-dimensional or line defect. How an electron near the line defect behaves? What are the influencing elements and parameters to consider? And secondly, the work engages the idea of confinement in homo-substrate, i.e., confinement created due to Ag(111) topography, and hetero-systems, i.e., confinement formed by the NaCl(100) adsorbate and Ag(111) substrate. Besides the effect contributed from a defect and confinement, the surface state of the electron depends on temperature, strain induced by the lattice mismatch [6], molecule adsorption [7], island size, and respective bandgap [6].

The work seeks to demonstrate credible results to enhance our learning about the surface electronic state spatially resolved near the 1-dimensional defect, which can help in fabricating nano-engineered devices serve varied purposes.

1.1. Basics of Scanning Tunneling Microscopy and Spectroscopy

STM is a scanning probe microscopy technique to get real space insight into samples in the picometer (pm) scale. The working principle of a scanning tunneling microscope (STM) is based on the quantum tunneling mechanism [5,8]. Thus, a very sharp metallic tip of spherical symmetry [2] is brought into the overlapping region of the wave functions with a conductive sample [8]. The distance between tip and sample is roughly kept between 5 Å and 10 Å (Fig. 1(a)) [4,8]. A bias voltage between the tip and the sample, i.e., the

voltage of the sample is measured with respect to the tip [9], results in the flow of tunneling current in the pA-nA range [2], and decays exponentially depending on the tip to sample distance (z) [3]. The tip is then moved over the sample in a raster fashion to probe the sample. The tunneling current is kept constant by adjusting the tip-sample distance (z) with an electronic feedback loop [5]. Since the tip-sample height dependence bestows STM with the capability to resolve molecule or substrate with high vertical resolution [2]. A change of the vertical height of 1 Å causes a change in the tunneling current by an order of a magnitude [3, 5, 10], or if the current is kept constant to within 2%, the gap width remains constant within 0.01 Å [3, 5]. For a symmetrical tip, 90% of the tunneling current flows through the apex of the tip and the adjacent atom on the surface [5].

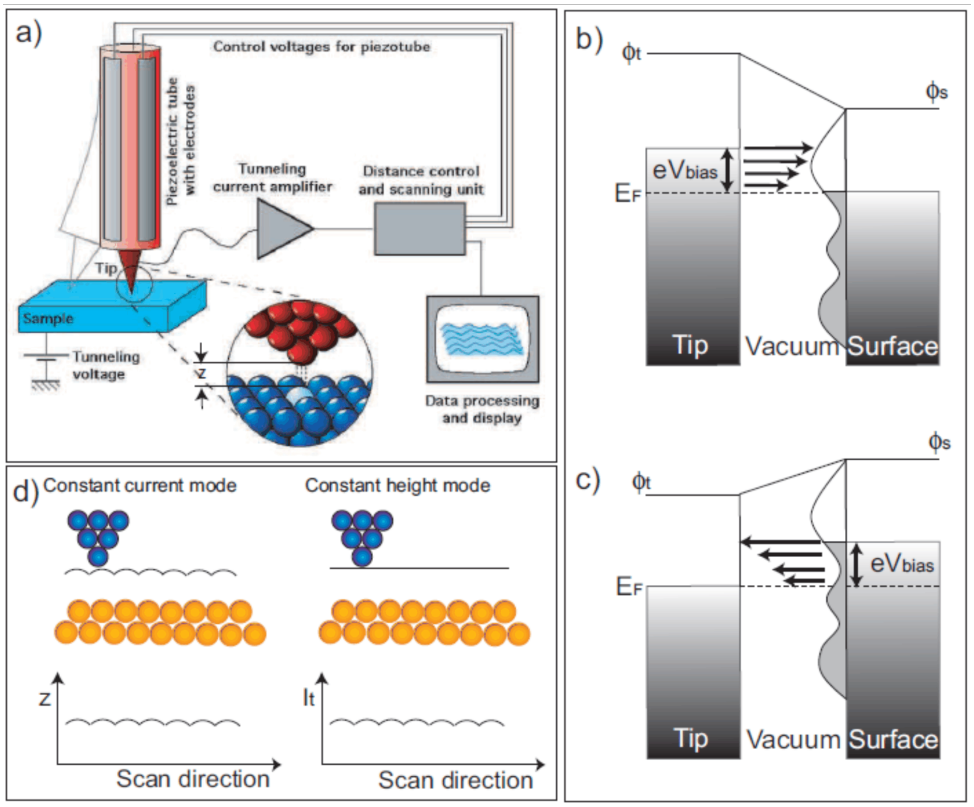

Figure 1: Schematic of the working principle of an STM. (a) The tip (red colour) is moved over a conductive surface (blue). The tip spatial movement is controlled via the z-piezo crystal through the feedback loop. (b) Electrons tunnel from the tip to the empty states (unoccupied states) of the sample with a positive bias voltage applied, and (c) electrons tunnel from the occupied states of the sample to the tip. (d) Different working modes of the STM. In(d) the tip is blue and conductive surface is yellow in colour, (*left pane*) constant current mode and (*right pane*) constant height mode [11].

The *modus operandi* for STM opt two possible techniques to probe; (i) constant current

mode, and (ii) constant height mode (Fig. 1(d)). In the constant current mode, the tip-sample height varies to keep the current constant via the feedback loop. This alteration in height is realized by applying a voltage $'V_z'$ to the z-piezo crystal of the STM [3]. Hence, during scanning, the tip remains in a constant height above the sample without touching or crashing into the surface. In the latter mode, the height is maintained constant over the surface. Hence, the quantity represented by the STM image is the electron density since the intensity of the image represents current changes [2], which are directly proportional to the adsorbate or surface underneath the tip. The negative bias applied to the sample with respect to the tip causes the electrons to tunnel into the tip, coming from the occupied states of the sample (Fig. 1(b)) [3], and if the sample is kept positive, the electrons tunnel from the tip to the unoccupied states of the sample (Fig. 1(c)) [3]. The occupied and unoccupied states are explored in the energy window defined between E_F and $E_F \pm eV$ [3,9,11]. Here, E_F is the Fermi energy and V is the bias voltage. Further, the tip scans the surface along the X and Y directions, the tunneling current is measured and recorded at each point of the digital XY matrix. The record of the feedback signal as a function of the tip lateral position results in a map of the molecule or surface topography.

1.1.1. Mathematical Equations

An STM image is the numerical transformation of current density under the tip, since the tunneling current I_t is then proportional to the density of states ρ of the surface at the tip position $\vec{r_o}$ [11]. Mathematically;

$$I_t(V) \propto \rho(\vec{r_0}, E) \tag{1}$$

To estimate the electron density underneath the STM tip, we integrate the current over the bias voltage [3]. The contribution to the tunneling current includes the tip wavefunction, surface wavefunction, and the transmission coefficient as a weight factor between them [3, 11]. The tunneling current I_t is thus expressed as:

$$I_t(V) \propto \int_{E_F}^{E_F+eV} \rho_t(E - eV)\rho_s(E)T(z, E, eV)dE \tag{2}$$

With the tip density of state (DOS) - ρ_t, the surface DOS - ρ_s, and the transmission matrix - T. The variables in parentheses signifies the dependence, i.e., tip - sample distance z, and the range of integration [E_F, $E_F \pm eV$]. According to Eqn.- 2, the tunneling current between tip and surface depends on three interconnected parameters; (i) the tunneling current I_t, (ii) the bias voltage V, and (iii) the tip - sample distance z [11]. Experimentally,

different sample properties can be probed by keeping one of the quantities constant in Eqn. 2. These relationships are listed in Tab. 1.

Table 1: Overview of the Spectroscopic Modes [1].

	Spectroscopy Mode	Constant	Surface Properties Measured
1	$I - z$	V	Local work function.
2	$V - z$	I	Electronic states above the vacuum barrier.
3	$I - V$	z	Local density of states (LDOS).

1.1.2. Scanning Tunneling Spectroscopy

Scanning tunneling spectroscopy (STS) establishes the relationship between the I - V parameter. To do so, the z - distance of the tip from the sample is kept fixed and the voltage is ramped across the system. This deciphers the electron local density of states (LDOS) over the occupied and unoccupied states of the respective system.

To evaluate the electron LDOS, Eqn.- 2 is differentiated with respect to the voltage to get the differential conductance, i.e., dI/dV.

$$\frac{dI}{dV} \propto \rho_t(E_F)\rho_s(E_F + eV)T(E_F + eV, eV, z) + \int_{E_F}^{E_F+eV} \rho_t(E - eV)\rho_s(E)\frac{dT(z, E, eV)}{dV}dE + \int_{E_F}^{E_F+eV} \rho_s(E)\frac{d\rho_t(E)}{dE}T(z, E, eV)dE \quad (3)$$

In the above equation Eqn. 3, a constant tip density of states ρ_t and constant transmission coefficient T is considered over the energy range [11]. Therefore, the derivative of the constant term results in zero. The two integrals in the Eqn.- 3 vanishes and the expression simplifies to:

$$\frac{dI}{dV} \propto \rho_t(E_f)\rho_s(E_f + eV)T(E_f + eV, eV, z) \quad (4)$$

The dI/dV in the Eqn. 4 is a good approximation to the electron LDOS [3, 11]. Experimentally, the detection of the dI/dV signal is achieved by the usage of a lock-in amplifier [3, 11, 12]. A small high-frequency sinusoidal signal V_{ac}, is added to the constant bias voltage V. This modulation causes a sinusoidal response in the tunneling current. The current then corresponds to the sum of V and V_{ac}. To achieve the differential con-

ductance, a first-order expansion via Taylor series delivers the required part [11]. To do so, a sinusoidal signal $V_{ac} = V_{mod}\sin(\omega t)$ is inserted into Eqn. 1 and later, expanded via the Taylor series:

$$I(V_{bias} + V_{mod}sin(wt)) \sim I(V_{bias}) + \frac{dI(V_{bias})}{dV}.V_{mod}sin(wt) + \frac{d^2I(V_{bias})}{dV^2}.V_{mod}^2sin^2(wt) + ... \tag{5}$$

By means of a lock-in amplifier we can extract the first harmonic frequency, which is proportional to the differential conductance signal dI/dV [11], i.e., the second part of the Eqn. 5. Here, the dI/dV is a function of electronic energy (eV) [**?**].

1.2. Substrate and Adsorbate

The substrate under consideration is a face-centered cubic (fcc) surface with a lattice constant of $a = 409$ pm. The (111) surface is formed by a cut along the [111] plane of the crystal (Fig. 2(a-c)) with a close-packed orientation of a hexagonal structure having six-fold symmetry [13, 14].

The studied adsorbate on top of the Ag(111) substrate is sodium chloride (NaCl), with a planar growth in (100) orientation on fcc metal surfaces [2, 13]. NaCl is an ionic crystal and has an fcc structure with a diatomic base i.e., Na^+ and Cl^- atoms, having a lattice constant $a = 563$ pm (Fig. 2(d-e)) [13]. NaCl, a decoupling insulating media has a bandgap of 8.9 eV within the first double-layer [13]. The apparent height in the STM image is voltage-dependent, i.e., (353 $\pm$ 45) pm between [-2, 2] V, indicates a double layer [6, 13]. Due to the broad bandgap, the electrons no longer tunnel through the NaCl and so, the apparent height is approximately the geometric height [10].

The orientation of the NaCl(100) over the Ag(111) substrate results in a line-like defect [13]. This effect couples to the first few top layers of the substrate atoms, resulting in compressional and tensile stress that displace the atom laterally. Due to these, the lattice constant for adsorbate and substrate deviates from their bulk values [15]. The exact calculation of the lattice constant remains a challenge. For a full layer, the Moiré patterns can be anticipated for evaluating the lattice constant underneath the respective pattern [13].

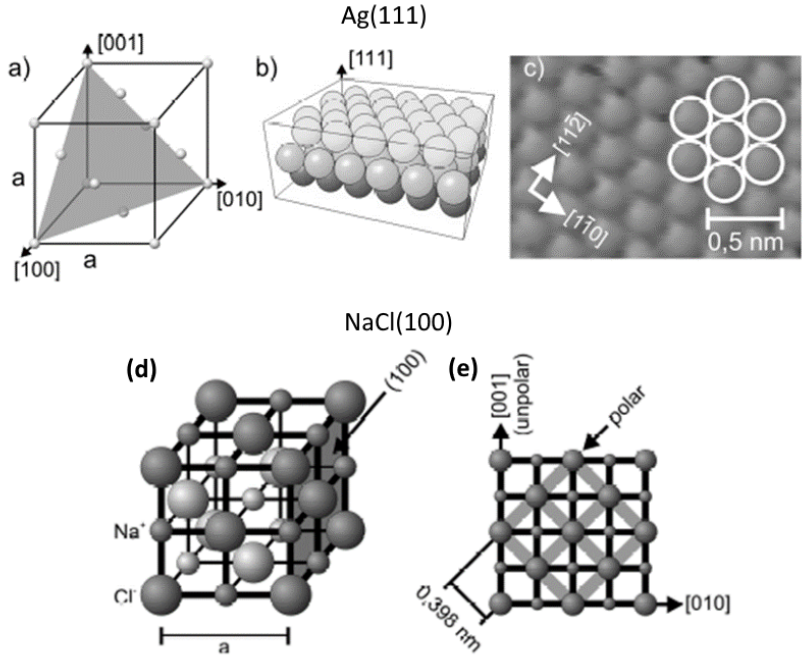

Figure 2: Ag(111) surface; (a) unit cell of an fcc crystal, the [111]-plane is marked in gray, (b) spherical model, and (c) STM image in atomic resolution (77 pA, 66 mV at 5 K). Ball and stick model of the NaCl(100) crystal (marked in picture Na^+ and Cl^-); (d) in volume structure, a denotes the lattice constant, the (100) plane is marked in gray and (e) (100) plane, the unit cells are marked in gray [10].

1.3. Defect

The presence of the defect in material science has unfolded certain physical systems that can withstand and demonstrate phenomena, where stoichiometrically balanced systems failed to acknowledge. For example, a photoluminescence effect due to nitrogen-vacancy (point defect) centres in diamond lattice and a similar point defect in hexa-boron nitride (h-BN) compound [**?**]. This defect induces the breaking of the symmetry that leads to distinct phenomena. In 1-dimensional defects, the Ag(111) surface accommodates various types of dislocations, including screw, edge [14], and Lomer-Cottrell dislocations [**?**]. When compared to other fcc metals, Ag has an exceptionally small stacking-fault energy so that the dislocations are observed more frequently in Ag films [**?**]. Furthermore, the adsorbate either chemisorbed or physisorbed perturb the top layer/s of the substrate via lateral dislocation of surface atoms that gives an impression of a ridge-like formation at the metal-insulator interface. In this thesis, 1-dimensional defects, i.e., slip plane dislocation, step edge defect, and strain-induced line-like defects caused by an adsorbate (Fig. 3) are investigated. Moreover, the adsorption of the NaCl induces a change in the direction (angle) of the step edge (Fig. 3(c)) [6].

The factors that contribute towards the defect studies include step reconstruction (Fig. 3(b)), surface roughening and corrugation, and terrace width [14], and confinement [16]. A disturbance in the periodicity of a crystalline surface structure leads to a change in its electron dynamics. For example, the terraces of inhomogeneous width affect the surface state of the electron [2]. Whereas, surface defects, even in a relatively small amount, potentially affect the processes at the surface like adsorption, diffusion, chemical reactions, catalysis, and thin-film growth [5,9,12,17]. Further, the lifetime of an electron is governed by the presence of a defect, adatom, and adsorbate. This strongly couple the surface state electrons to bulk, and thus reduces the lifetimes [17].

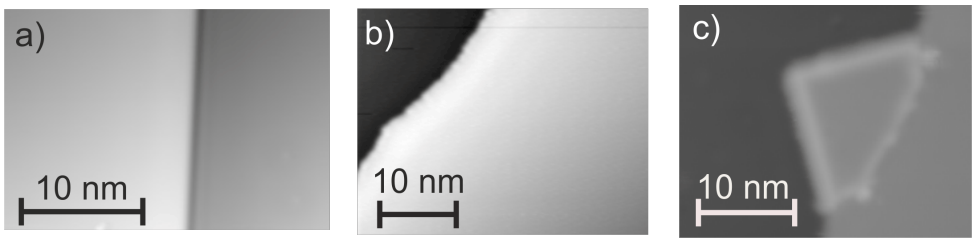

Figure 3: STM images of 1-dimensional defects. (a) Slip plane dislocation and (b) step edge defect on Ag(111) surface. Tunneling parameters: -0.2 V, 1 nA, and 5 K. In (c) NaCl(100) adsorbed at step edge of the Ag(111) surface. Tunneling parameters: -0.3 V, 0.2 nA, and 5 K. The step height in (a) and (b) is 0.24 nm and the height of the NaCl(100) island is 0.247 nm at -0.3 V.

1.3.1. Slip Plane Dislocation

Slip plane or slip step [1] dislocation forms due to orthogonal movement of the atoms to compensate tensile strain in the Brillouin zone of the bulk [18]. This strain at the surfaces occurs because the gap in the Brillouin zone of the bulk displaces the atomic plane perpendicular to the direction of close-packed atoms (Fig. 4). In Fig. 4, there is a perpendicular shift in bonds across the atomic plane from **1** to **2** and so forth, with respect to [111] plane results in the formation of a slip plane in $\langle 110 \rangle$ [1, 18]. The release of strain onto the surface results in a step edge formation of the highest symmetry on Ag(111) with a step height of 0.24 nm [14].

1.3.2. Step Edge Defect

Step edges are formed during the sample preparation, i.e., an outcome of thermodynamic processes. This type of defect has 'atomic-scale roughness' (Fig. 3(b)) [14], containing kinks, step vacancy, and step adatom [5]. The properties of substrate and adsorbate are strongly influenced by the presence of a step edge. At a step edge, properties like molecular geometry, chemical activity, diffusion, and crystal growth [14] may differ from

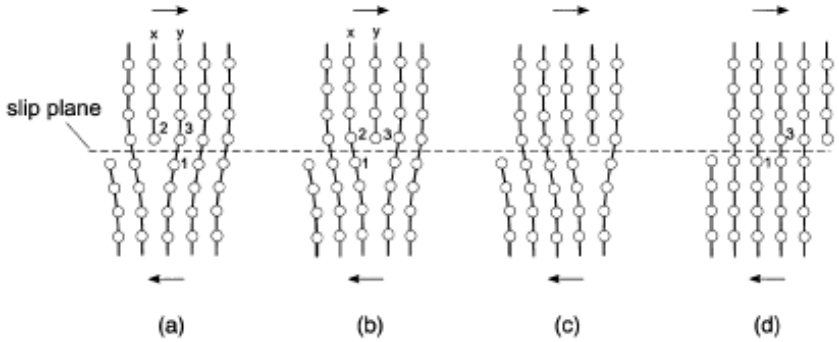

Figure 4: Formation of slip plane. Movement of an edge dislocation. The arrow indicates the applied shear stress. The number represents atom planes, that shift the bond and move the plane to compensate the force [18].

those observed on the terrace. The roughness at the step edge exhibits a polarity effect, which makes step edges a highly preferred adsorption site compared to the terrace.

1.3.3. Adsorbate Induce Line Defect

The presence of the decoupling layer creates 'misfit-induced strain' (Fig. 3(c)), which causes the lattice constant to be different from the bulk value [19]. Secondly, the site of adsorption, i.e., terrace or step edge, determines the specific orientation of the decoupling layer and height. This directly affects the electron LDOS and the latter causes charge redistribution around the respective system.

1.4. Surface State

The nano-cosmos of the 'surface' is defined by the 'quasiparticle', a fundamental concept in condensed matter physics [17]. 'What determines the local environment of the quasiparticles, and the change introduce in the behavior of the quasiparticle?'. Qualitatively speaking, the lifetime determines the mean free path of the quasiparticle [17], i.e., the excitation and decay processes, and is influenced by the physical environment of a system. Edge and screw dislocation, surface reconstruction, presence of defects on the surface and in the bulk, and adsorbate constitute different environments towards the quasiparticle. Therefore, these impact the electronic surface states [17] and result in different lifetimes of the electrons [14].

A break in the surface symmetry [16] instills a new electronic surface state with open tangling bonds. This leads to a change in the electron dynamics on the surface relative to the bulk. Since these features are solely found at the crystal surface, the electrons of these states behave like a 2-dimensional electron gas (2DEG). One can further define the elec-

tron behavior in terms of many-body physics, as electrons undergo different interactions and scattering, it redefines 'energies' at each site of interaction. The scattering processes include electron-electron, electron-phonon, and electron–defect scattering processes [1].

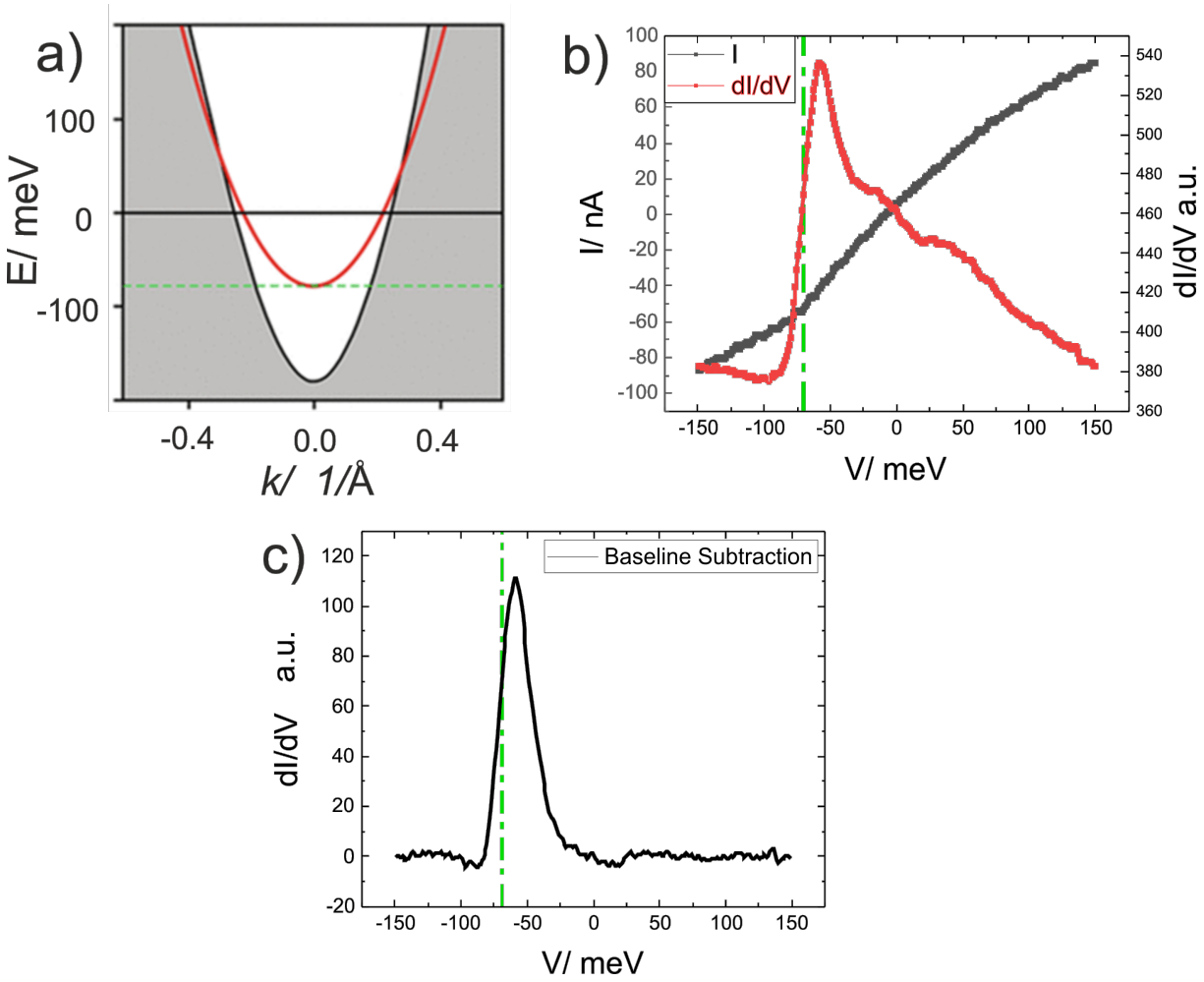

Figure 5: Schematics of the onset of the surface state. (a) Energy distribution in k-space. Here, gray represents bulk states and red for the surface state. The dotted green line passes tangentially at k=0.0 (1/Å) of the surface state defines the onset of the surface state. In (b) the STM/STS spectrum corresponds to the surface state plot in (a). The green dotted line transect the I-V and dI/dV at the onset of the surface state. This can be indicated via kink in the I-V spectrum. And, in (c) a baseline planar subtraction is done on dI/dV vs V representing a single onset peak.

The studies are focused on the Shockley surface state metal. The Shockley state is formed in the bandgap of the bulk states projected along the $\vec{\Gamma} - L$ line [3, 7, 16]. In the Brillouin zone, $\vec{\Gamma}$ represents center - (0,0,0) and L represents the center of a hexagonal face [5]. An electron present in the minimum band of the Brillouin zone, i.e., $\vec{\Gamma}$, see an energetic barrier by vacuum above the surface (Fig. 5(a)) [15]. Further, the transfer of an electron

into the bulk comes at the loss of energy or momentum [3]. Therefore, such an electron is free to move along the surface in a delocalized Shockley surface state [16]. For Ag(111), the minimum band is at an energy of (-65 ± 3) meV [7,13,14].

1.4.1. Surface State of an Insulator

The presence of an adsorbate introduces a difference in bandgap (Fig. 6) and lattice mismatch, which results in different scattering processes, affects the lifetime (τ) and the effective mass (m^*) of the electron [4,10,17]. The adsorbate for an incoming electron can act as a scatterer or an absorber (black scatterer [2]), and in confinement behaves like a step-potential.

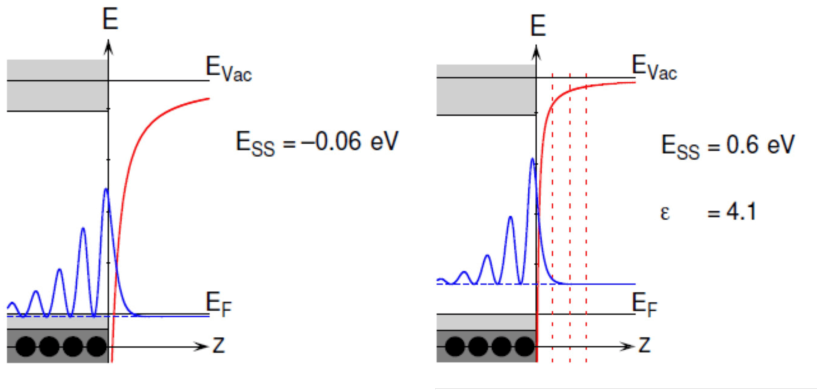

Figure 6: The presence of a dielectric layer on the Ag(111) shifts the surface state above the Fermi energy. (a) Without a dielectric layer and (b) covered with a dielectric layer with ε(E) = 4.1. Here, the red colour mark represents the surface and interfacial potentials, and the blue for exponential decay into vacuum and bulk. The bottom marks a slab-like structure containing silver atoms in black [10].

1.4.2. Surface State Parameters - Physical Interpretation

The electrons present underneath an STM tip hold characteristic information about the adsorbate and substrate system [2]. To quantize the information of electronic surface state, certain parameters have been classified over time that corresponds to the minimum band of the Brillouin zone [9]. In STM/STS studies, it is evaluated using the local density of states (LDOS) or differential conductance via the *I-V* characteristic curve (Table 1 Pg. 4). The kink in the *I-V* spectrum indicates the onset of the surface state or onset energy (or voltage) (Fig. 5(b)). Besides this, a couple of more peaks are vibrant at higher energies that occur near the defect [?] and in the confinement [?]. Though, on a bare surface, only one single peak is seen for the onset of the surface state (Fig. 5(c)). Our thesis resides to

identify the change in onset energy as the primary task, whereas all other peaks signify different electronics bands and scattering processes. The parameters to evaluate STS includes; (i) onset energy (E)- middle of the rise of the first onset peak, (ii) $\triangle$ (pronounce *del*) - the width or broadening of the onset peak due to the processes, and (iii) **I** - the intensity of the electron population, calculated via the height of the onset peak (Fig. 7).

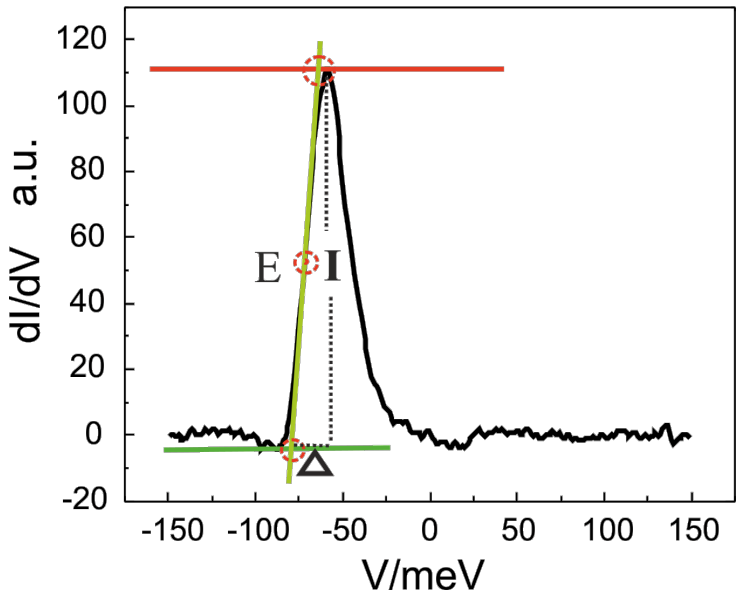

Figure 7: Surface state parameters. A dI/dV - V characteristics curve of the Ag(111) substrate. Here, E represents the onset energy, $\triangle$ is the broadening, and **I** is the intensity.

Mathematically, the onset voltage (E), broadening ($\triangle$), and intensity (**I**), following relations are recognized for the evaluation of the surface state [10].

$$E = x_{onset} = \frac{1}{2}(x_{max} + x_{min}), \tag{6}$$

$$\triangle = x_{max} - x_{min}, \tag{7}$$

$$\mathbf{I} = y_{max} - y_{min}, \tag{8}$$

The broadening of the onset energy is affected by the modulation voltage (V_{mod}) and temperature (T) [19]. To reduce the effect in broadening ($\triangle$), the following calculation is employed to evaluate the intrinsic broadening,

$$\triangle_{intr.} = \sqrt{\triangle^2 - (\frac{\pi}{2}.eV_{mod})^2 - (6.k_BT)^2} \tag{9}$$

Here, k_B is the Boltzmann constant. And the formula for the lifetime (τ) is,

$$\tau = \beta \cdot \frac{h}{4\triangle_{intr.}}, \tag{10}$$

For above, h is Planck's constant, and β is a factor close to unity that measures the extent to which the tunneling state couples to lifetime limiting processes [10, 17]. With beta equals 0.89, the τ has been reported 120 fs [10, 16]. However, in the presence of slip plane dislocation >80 fs, a lower limit is because of the instrumental broadening [14].

Final remarks, the work in the thesis employed these basic relations to sketch the electron behaviour and dynamics near the 1-dimensional defect and in confined spaces.

2. Experimental Setup and Methodology

The experiments are performed in a home built low-temperature STM under ultra-high vacuum (UHV) conditions (Fig. 8). The base pressure is $\leq 2.0 \cdot 10^{-10}$ mbar. The Ag(111) (*MaTeck, Jülich, Germany, surface orientation better than 0.1°; no impurity detectable by XPS* (*Phoibos 100, SPECS, Berlin, Germany*)) surface is cleaned by several cycles of sputtering and annealing. The sputtering is performed via an ion gun (*IQE35 from SPECS, Berlin, Germany*) with Ne^+ ions at $p_{Ne} = 3 \cdot 10^{-5}$ mbar for 3 min to 60 min. After each sputtering, the sample is annealed at 823 K - 923 K for 6 min. Aiming for large terraces separated by step bundles [6]. The sample is cooled with a cooling rate of 5 K/sec down to 300°C initially, and then cooled at a reduced rate of 1 K/sec down to 80°C. The NaCl powder (*Fluka Chemika; purity* $\leq 99.5\%$) is purified in an external setup of a dry furnace. It is degassed for more than 10 hour at 200°C. Subsequently, the NaCl is filled into a molybdenum-coated ceramics crucible and is mounted in a commercial evaporator (*type EFM from Omicron, Taunusstein, Germany*). It is further degassed in a molecular chamber for 2 and 3 days at a heating power of 1.5 W. It is validated that the water content is below the detection level of the mass spectrometer (*QMA 200 from Pfeiffer Vacuum, PT M25 252*). Afterward, the cleaned NaCl is deposited via heating at 3 W and maintaining the current flux between 0.25 nA - 6 nA. A constant deposition rate of 0.02 monolayer(ML)/min, which is maintained for up to 12 min. The deposition temperature of the sample is held at room temperature (298 ± 6) K, such that the molecules are mobile enough to reach the step edges and form islands. After deposition, the substrate is cooled abruptly via liquid helium flow through the manipulator ≈ 30 K (Fig. 8). The sample is then transferred into the STM. Measurements are performed at 5

K. The topographic images are taken in constant current mode. To take a dI/dV curve, the feedback loop is opened once and the tip is kept at a fixed height. The voltage is then gradually ramped from -300 mV to 300 mV range.

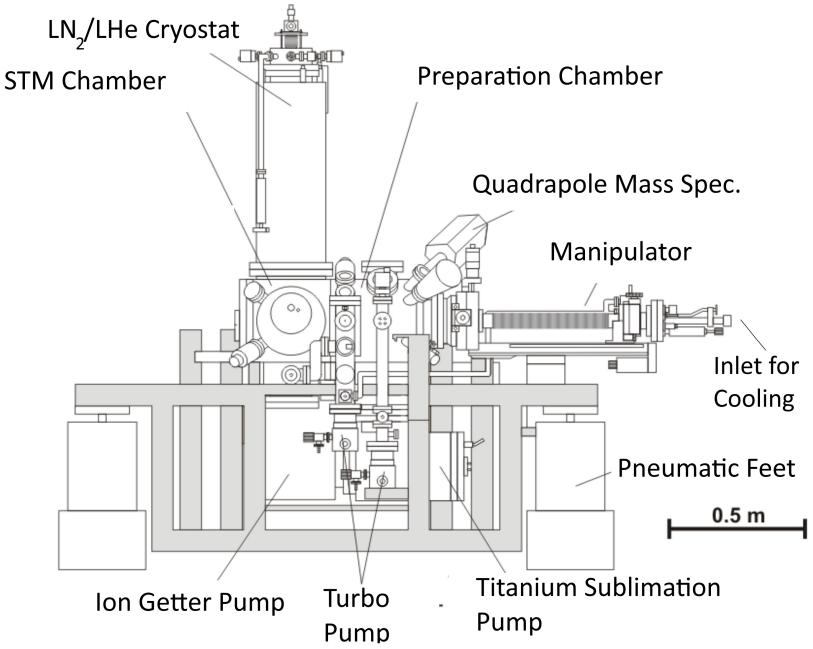

Figure 8: A pictorial sketch of the STM with all basic operational instrumentation [11].

2.1. Error in Experimental Measurement

Working under such experimental conditions comes at the cost of instrumental limitations and errors. These include mechanical (vibrations), electronics and electrical, and thermal connected noise. Besides the STM system limitations, the adsorbate-substrate system also affects the measurements. To overcome these artifacts, STM contains pneumatic feet with sand-boxes to dampen and reduce the mechanical vibrational frequencies (Fig. 8). For electronic and electrical noise reduction, appropriate filters and wires are used. For temperature connected noise, e.g., thermal drift and creep caused by the z-piezo, this leads to the spectra recorded at a specific point in time on the substrate to undergo displacement (Fig. 9). A simple calculation is done to retrieve the initial point. However, to have high thermal stability, an active thermal drift compensation technique can be used [12].

Regarding tip-related errors, tip convolution at higher energy [**?**] and unwanted variation in tip–sample distance at constant parameters [14]. And calculations regarding the onset energy, broadening ($\triangle$), and intensity (**I**) are evaluated using two different computational methods - MATLAB and OriginPro Software. Comparative error graphs are presented

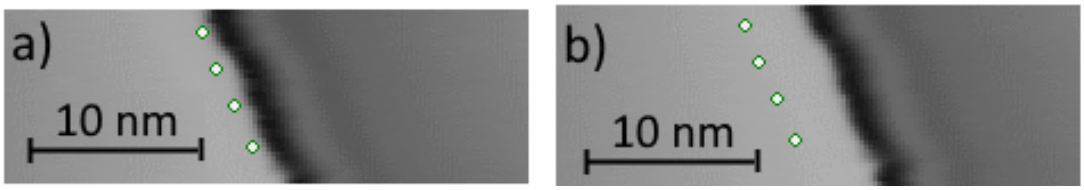

Figure 9: Creep induced displacement. The z-piezo stage undergoes a shift in displacement due to creep. This makes the STS spectrum record at some other spatial coordinates on the substrate.

for both computational methods for all STS parameters (Fig. 10).

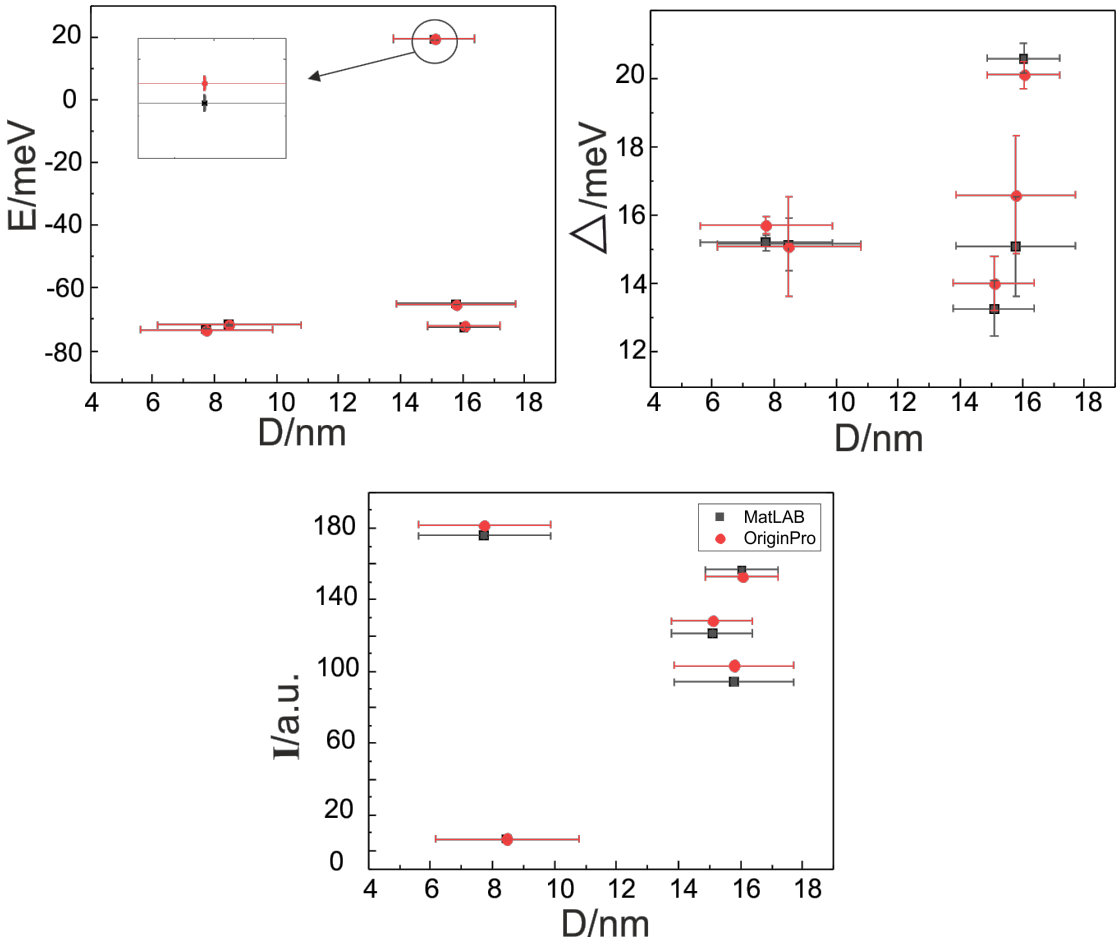

Figure 10: Error computation for individual STS parameters. (a) Onset voltage (E/meV) vs distance (D/nm), (b) broadening (△/meV) vs distance (D/nm), and (c) intensity (**I**/arb. unit) vs distance (D/nm). In (a) a square box has been drawn to signify the minute change in the y-axis. The black marker represents calculation done with MATLAB and red with OriginPro Software.

2.2. Methodology

The studies undertook 1-dimensional defect in Ag(111) substrate and NaCl(100) adsorbed on Ag(111) substrate. Three defect cases will be discussed regarding Ag(111) and four cases regarding NaCl(100)-Ag(111) system. For the measurements on Ag(111), the tunneling parameters are -0.2 V, 1 nA at 5 K and for the NaCl(100) on Ag(111) system, the tunneling parameters are -0.3 V, 0.2 nA at 5 K. Each section leads to a different and the distinct interpretation is given that the phenomena seen are independent of the previous case.

3. Literature Review

Noble metal surface states have been the focus of experimental interest for over decades [4]. The electrons occupying surface states on the close-packed face form a 2-dimensional nearly free electron gas [16], in the bandgap of the bulk state, projected along $\vec{\Gamma}$-L line (Fig. 5(a)) [3,7,16]. The metal-specific electronic surface state depends on the presence of different s, p, and d - bands. It gives a spectroscopic signature in the first-order derivative of the I-V characteristic curve (Fig. 5(b)) in STM/STS studies. The tunneling current is measured at a fixed height over a range of bias voltage, demonstrating the occupied and unoccupied state of the system (Fig. 1(b-c)) [16]. The onset of the energy is dictated both by the presence of a step [2, 15, 16], dependent on terrace width [15], and defects [1, 6]. These sites open different scattering channels leading into the bulk [16]. Further, the scattering leads to a change in path-mediation and so, affects the lifetime of the quasiparticle. These scattering phenomena can be categorized into electron-electron (e-e), electron-phonon (e-ph) and electron–defect scattering (e-def) cause a loss of energy or momentum and a change in direction [1].

The quasi-two-dimensional electron gas is confined between vacuum barrier and a projected gap in the bulk density of states as referred to as Shockley type of surface state [15, 20]. Further, it offers a higher density of electrons at the surface that reduces the lifetime of the electronic excitation, i.e., typically in the femtosecond range [4, 7, 14]. An adsorbate or a defect alters the symmetry of the surface and act as an absorber (black scatterer [4, 7]) [16] or a scatterer for incoming electrons, which reduces the lifetime of the electron. For example, metallic scatter Fe on W(110), and Cu stripes on stepped W(110) and Mo(110) [16], non-metallic impurities, e.g., carbon impurities on V(0001) [3], insulator like ZnO films on Au(111), and NaCl(100) on Ag(111) [6]. Moreover, structural topography shifts the surface state towards the Fermi energy, e.g., near step edges and terraces with shorter widths [3]. Altogether, scattering phenomena strongly couple

the surface state electrons to bulk states (electron-electron scattering) or excite a surface vibration (electron-phonon scattering) or result in electron–defect scattering [1, 17]. However, in the absence of defect scattering, two processes limit the lifetime; inelastic electron-electron scattering and electron-phonon coupling [17]. The scattering processes are not only limited to a defect and an adsorbate, but the confinement geometry exhibits similar phenomena. In confinement studies, either due to geometrical defect or purpose-built structured barriers facilitate the principle of 'particle-in-a-box' [16] or 'cylinder' [3]. Here, particle represents an 'electron' and 'box' or 'cylinder' is subject to structural topography of the substrate-substrate (homo) or adsorbate-substrate (hetero) confinement systems [19]. A common example of the adsorbate-substrate hetero-system is the "quantum corrals" [16], by constructing an atomic-scale Fe metallic barrier to confine the surface state electrons [3, 16] laterally [4]. The qualitative behaviour of the quantum corrals can be explained by modeling them as simple hard-wall "electron boxes" [10, 16]. For homo-confinement systems, Ag embedded stacking-fault tetrahedrons (SFT) nanostructures on Ag(111). A triangular shape confined space quantized the electron laterally. The lateral confinement leads to splitting up the surface state energy band into a series of discrete energy levels. However, only a proper combination of the confinement or structured barrier can yield a detectable number of quantized eigenstates [**?**].

The observed adsorbate NaCl has an 8.9 eV bandgap with a bipolar ionic nature and brittle structure even in a thin layer [6]. Its adsorption to less brittle Ag(111) substrate results in lattice mismatch and reconstruction at the step edges. This induces strain among the top layers of the metal surface near the interface [19]. It has been an established fact that NaCl(100) islands have a different percentage of mismatch along the two planar axes, i.e., $\langle 110 \rangle$ and $\langle 112 \rangle$, which makes the Ag(111) undergo reorientations and creations of kinks and changes the step edge direction (Fig. 3(c)) [19]. The percentage mismatch along $\langle 112 \rangle$ - direction results in an 11% lattice mismatch and whereas, NaCl$\langle 110 \rangle$ fits well to Ag$\langle 100 \rangle$ [15]. As the STM imaged only the anions, the measured value for chlorine anion is (389 $\pm$ 6) pm similar to the value determined for larger islands, the other distance is (373 $\pm$ 7) pm. With (559 $\pm$ 4) pm and (513 $\pm$ 8) pm in bulk, the lattice constants differ in the two perpendicular directions [6]. A minute level of top layer atomic displacement and lattice mismatch results in line defect and induces scattering phenomena.

On the Ag(111) substrate, the surface state of the electron exhibits one clear maximum at (-65 $\pm$ 3) meV (Fig. 5(c)) [13, 14]. The presence of an upper and a lower terrace in slip plane and step edge defect, and the interface between adsorbate-substrate engages different scattering channels for the electron [**?**, **?**, 17]. Whereas in the confinement, different

surface electronic bands are introduced as per the geometry of the confine system. Since an electron undergoes different interactions, results in different lifetimes (τ) and effective masses (m^*) [6].

Scattering of surface state electrons from defects produces interference patterns known as electron standing waves. The electron standing waves can be directly observed even in normal STM images when acquired at lower biases close to the Fermi energy on Ag(111) [16]. At higher biases, however, the tunneling current represents a weighted integral over a range of energies, and the oscillatory signal is smeared out. This is related to the increasing influence of tip convolution effects with increasing energy [**?**, 16]. Interference of the scattered wave with an incoming wave gives rise to an oscillatory variation of the local density of the surface state in the vicinity of scatterers. Therefore, the surface LDOS is obtained by taking into account the various possible scattering paths an electron can make before returning to the tip [16]. Which results in an interference term to the LDOS. Near the defect and adsorbate, electron-defect scattering followed by elastic electron-electron and electron-phonon scattering are dominant processes. In the defect scattering, electrons undergo collision that results in lateral displacement over the surface. This lateral coverage of the surface electron is dependent upon the nature of the defect or adsorbate. One can expect, enhanced coupling to underlying bulk states of the Ag(111) surface at higher energies [**?**]. This electron either decays via intraband transition (bulk states) or interband transition (electron-phonon scattering) [1, 17]. This transfer of electrons from the surface state to the bulk states leads to a decrease in the lifetime of the electrons in the surface state [10] and the loss of momentum of the electron scattering into the bulk at the defect site is compensated by the electron-defect scattering [17]. However, some reservation exists for the scattering process in the confinement. Confinement behaves differently and directed us to capitulate the observation in an independent paradigm regarding the surface state of the electron. In confinement or structured barrier studies, at higher energies, bulk states and surface states are governed by the geometry of the system [**?**] and give rise to new energy eigenstate [1]. This affects the scattering processes, energy eigenstate, and conservation of mass. This leads to different surface electronic states within the confinement. This affects the electron present outside the confinement to act differently than the one present inside the confinement [16]. Thus, within confinement, different decay time for the electron is evaluated, and thus, leads to specific spectroscopic signature and processes.

4. Results and Discussion

As the structural topography of each defect varies, so is the processes and respective STS parameters. Therefore, we divide the thesis into two sections:

Section I

The surface state electrons are affected by the structural change in the 1-dimensional defects in Ag(111) substrate. This section solely discusses the defects that exist on the surface. It includes,

1. Slip plane dislocation.
2. Step edge defect.
3. 2-D confinement system.

Each case study contains three parts; (i) experimentation and methodology, (ii) trends observed in the STS parameters, i.e., onset energy, broadening, and intensity, and (iii) physical interpretation of the trends.

4.1. Slip Plane Dislocation

Recording of the STS spectra started from the upper terrace (left) with ∼0.5 nm distance between each dI/dV and continued towards the lower terrace (right) (Fig. 11(a)). Total recorded STS spectra are 40 data points, half of them on each terrace. The most negative value in the graphs indicates the starting point of the STS spectrum. Here, the origin (x = 0) is at the slip plane dislocation. In Figure 11(b-d), the red dotted vertical line signifies the correction made to adjust the creep of the piezo crystal. This correction is the right displacement of the axis by 0.5 nm.

The values extracted for the onset energy, broadening (△), and intensity of the electron population (**I**) from the STS spectra for the upper and the lower terraces exhibited an asymmetrical trend. Referring to Fig. 11(b-d), each graph contains an arrow, indicating the change in the surface state of the electron with respect to the line defect ($x = 0$). As STS took near the line defect ($x = 0$), the onset of the surface state shifts upward to the Fermi energy, and the broadening of the onset energy (△) is doubled (Fig. 11(b-c)). Whereas, the intensity of the electron population (**I**) is first increased and then decreased, followed by another sharp decline in electron population near the defect (Fig. 11(d)-*marked with red and yellow arrows*). Similar results were reported for the slip plane dislocation in [14].

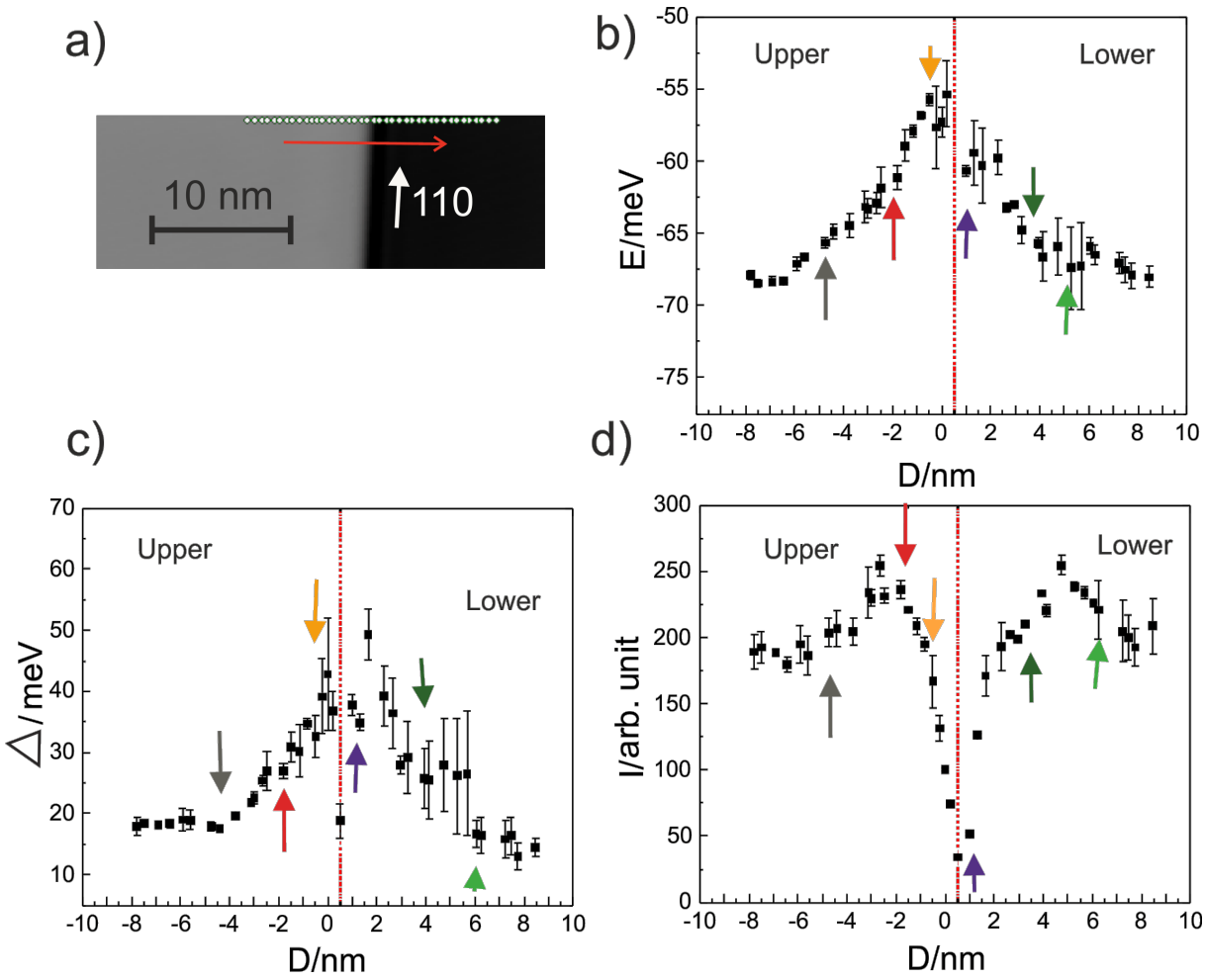

Figure 11: STS parameters plot of the slip plane dislocation. (a) STM image of the slip plane dislocation. Tunneling parameters: -0.2 V, 1 nA at 5 K. (b) Onset energy (E/meV) vs distance (D/nm), (b) broadening of the onset energy (△/meV) vs distance (D/nm), and (c) intensity (**I**/arb. unit) vs distance (D/nm). Here, the red dotted line is drawn at 0.5 nm due to the creep. A direction of the arrow in (a) means the starting of the STS spectrum from the left/upper terrace to the right/lower terrace. Different colour arrows are marked in each plot to indicate the change in LDOS.

The physical interpretation for the trends obtained is different for the upper and the lower terrace. On the **upper terrace**, the influence from the line defect on the onset energy first occurred between -4 nm and -5 nm (Fig. 11(b)-*gray arrow*), and the second shift in an upward trend with a greater slope towards the Fermi energy occurred around -2 nm from the slip plane dislocation (Fig. 11(b)-*red arrow*). At the origin, the onset energy is (-56 ± 2) meV (Fig. 11(b)-*yellow arrow*). The attenuation in onset energy over the distance of 6 nm is (12 ± 2) meV. In the broadening of the onset energy, the first change occurred at -4 nm (Fig. 11(c)-*gray arrow*), the next one around -2 nm (Fig. 11(c)-*red arrow*), and the maximum processes occurred next to the dislocation (Fig. 11(c)-*yellow arrow*). The

average change in broadening of the onset energy is (25 ± 5) meV. A similar pattern is followed in the intensity of the electron population. The first change occurred at -6 nm and then, between -2 nm and -3 nm from the dislocation (Fig. 11(d)-*red arrow*). Here, the maximum intensity is (254 ± 8) arb. unit calculated at -2.6 nm from the dislocation. Between -2.6 nm and ≈-1 nm from the dislocation, a first drop in the slope of the electron population and later, followed by a sharper drop between ≈-1 nm and the dislocation is seen in the plot (Fig. 11(d)-*yellow arrow*). The lowest calculated value for the intensity at the dislocation is (34 ± 4). A seven-fold reduction in the electron population is seen over a distance of 3 nm from the dislocation. Relatively speaking, ≈85% ± 3% drop in electron population near the dislocation. Whereas for the lower terrace, to avoid repetition, the first process occurred between 5 nm and 6 nm (Fig. 11(b-d)-*light-green arrow*), the second one around 3 nm (Fig. 11(b-d)-*dark-green arrow*), and the last processes occurred at ≤1 nm (Fig. 11(b)-*purple arrow*). A similar percentage drop in electron population is seen for the lower terrace.

To interpret these numbers, scattering and diffusion processes are dominant with variable intensity over each terrace. An electron present on the upper terrace experienced two effects at the edge dislocation. Firstly, the Smoluchowski smoothing effect and secondly, the bulk-surface mixing underneath the dislocation. The Smoluchowski effect leads to the creation of a dipole at the edge dislocation due to charge-redistribution [20]. The top of the edge has a positive polarity and the bottom of the edge has negative polarity. The positively charged edge now repels the incoming electron and partially acts as a barrier. This leads to electron scattering back onto the upper surface. Whereas, the presence of the bulk-surface mixing underneath the dislocation affects the electron population present on the upper terrace up to -2.6 nm. A dropped in the electron population is seen as we approached near the dislocation. In brief, the trends observed in the STS parameters with different peaks, slopes, and drop identify the following phenomena; (i) The electron-electron scattering leading into the bulk affects the LDOS up to -2.6 nm from the dislocation, (ii) the Smoluochowski smoothing effect is less pronounced than the bulk effect, and (iii) major of the processes occurring near the dislocation is possibly due to bulk participation and distance (-2.6 nm) away from dislocation gives interband transition or electron-phonon scattering due to the Smolouchowski smoothing effect which leads to charge distribution. Altogether, to spatially resolve the processes on the upper terrace, the upper limit from the defect extends up to -6 nm, whereas the lower limit exists at the edge dislocation.

Next, the lower terrace holds many of the scattering phenomena due to the presence of

the bulk-surface mixing leading to intraband transition. Secondly, the step height of the slip plane act as a soft wall. This affects the incoming electron to back-scattered with greater probability (∼70%). Unlike the upper terrace, where the Smoluchowski smoothing effect dominates the back-scattering phenomenon. This soft-wall leads to electron-defect scattering. Moreover, the loss of an electron into the bulk is compensated by the electron-defect scattering. Therefore, we expect the electron-electron and electron-defect scattering is dominant processes to occur at the defect side. On close analysis, in Fig. 11(c)-*dark-green arrow*, the bulk participation has a greater effective length in the lower terrace over the LDOS. Relatively speaking, the bulk participation length is increased by ∼75% compared to the upper terrace. The drop in the electron population occurred at ≈ 4.6 nm. One more observation regarding the processes, i.e., broadening of the onset energy. In Fig. 11(b)-*between dark-and-light green arrows*, the recorded values have greater uncertainty, i.e., perturbations. And a similar region in Fig. 11(d) shows the electron population is decreasing in this region. The influence from the bulk is minimal or next to none. The electron excitation and decay are dominated in this region via electron-phonon scattering (interband transition). This speculation is prone to error, but in the absence of the defect, electron-electron scattering and electron-phonon coupling (vibration) become active processes.

4.2. Step Edge Defect

In this case, three different datasets across the step edge were recorded with each containing 10 STS spectra from the upper terrace (left) towards the lower terrace (right) (12). The trends are partly similar to that of the slip plane dislocation. The factor that contributes towards the deviation is the presence of an 'atomic-scale roughness' at the step edge (Fig. 3(b) and Fig. 12) [14].

In Fig. 13, each dataset has shown deviations in the STS parameters. Only dataset-(ii) and dataset-(iii) are partially similar in the onset energy and the broadening of the onset energy (Fig. 13(a-b), 2^{nd}-3^{rd} row). For the electron population, dataset-(i) and dataset-(ii) are partially similar (Fig. 13(a-b), 1^{st}-2^{nd} **row** and 3^{rd} **column**). Common features like a rise in onset energy towards the Fermi energy, an increase in the broadening of the onset energy, and a decrease in the electron population into the bulk are seen near the defect. A brief table (Tab. 2) has been presented for the change seen in STS parameters for the respective terrace measured from the distant datapoint to the step edge defect. This tabular summary helps in deciphering the change in LDOS spatially from the step edge defect.

The occurrence of maxima and minima in Fig. 13(a-c,i-iii) indicates the change in the electronic states. For the upper terrace, the onset energy is shifted upwards to the Fermi

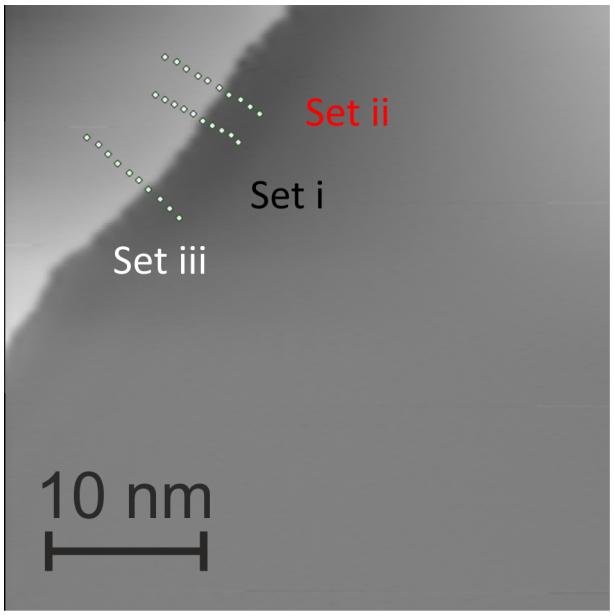

Figure 12: STM image of a step edge defect. Three datasets across the step edge. The step height of the step edge is 0.24 nm. (Tunneling parameters: -0.2 V, 1 nA, and 5 K).

Table 2: The change in STS parameters for the upper and the lower terrace near the step edge defect.

STS	**Set-i**	**Set-ii**	**Set-iii**	**Terrace**
E/meV	18 ± 3	13 ± 2	9 ± 1	Lower
(Onset energy)	18 ± 1	28 ± 1	20 ± 2	Upper
△/meV	104 ± 5	25 ± 3	26 ± 4	Lower
(Broadening)	46 ± 2	102 ± 8	34 ± 12	Upper
I/arb. unit	195 ± 6	346 ± 7	77 ± 6	Lower
(Intensity)	150 ± 5	165 ± 4	12 ± 4	Upper

energy in an unsymmetrical and disproportioned manner (Fig. 13(a, i-iii)). The explanation for such phenomena is due to the presence of roughness at the step edge. This gives rise to kinks, acting as a scattering center for incoming electrons, and leads to unbalance and asymmetrical charge redistribution across the rough step edge. Therefore, this results in spikes in the onset energy, an abrupt shift in the broadening, and a sharp decrease in the electron population near the step edge defect (Fig. 13(a-c,i-iii)).

Once again, the lower terrace holds a couple of more processes than the upper terrace. The presence of a 1-dimensional defect leads to bulk-surface mixing, which leads electrons into the bulk. Further, the Smoluchowski smoothing effect hinders electron diffusion from the upper surface to the lower. The sole processes occurring in the lower terrace are attributed to the presence do the defect. The loss of an electron, i.e., the momentum,

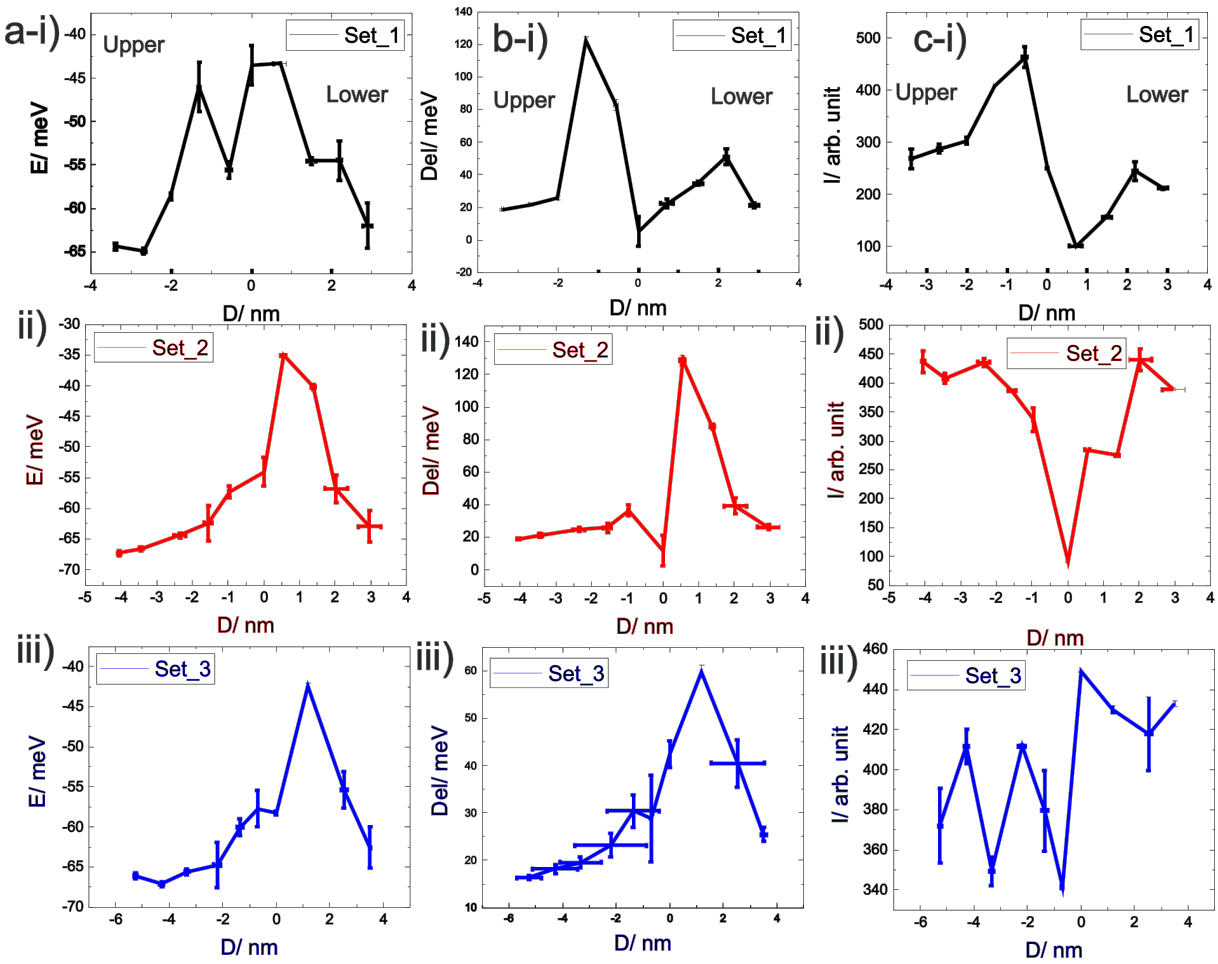

Figure 13: STS parameters for the datasets-i, ii, and iii. (a) Onset energy (E/meV) vs distance (D/nm), (b) broadening of the onset energy ($\triangle$/meV) vs distance (D/nm), and (c) intensity of the electron population (**I**/arb. unit) vs distance (D/nm). The step edge defect is considered at origin (x=0). The negative axis represents measurement took on the upper terrace and the positive axis as lower terrace.

is compensated by the electron-defect scattering. In the lower terrace, a back-scattered electron from the step edge forms a standing wave pattern. Though, due to the roughness of the step edge, we expect that lateral relaxation length will be lesser than the slip plane dislocation (Sec. 4.1 Fig. 11). Relatively speaking, the electron population in the lower terrace in this case (Fig. 13-*last column*) is ≈80% higher than that of the slip plane dislocation (Fig. 11(c)). Referring to Fig. 13-*second column*, the spread of data for broadening of the onset energy is irregular. This can be due to an experimental error. At the end, **Appendix - A** (Pg. 50) contains the dI/dV vs V graphs for all these datasets to ensure the credibility of the work. However, on the comparative ground to the slip plane dislocation, more than a two-fold increase in processes has occurred in the step edge defect.

A comprehensive table (Tab. 2) is drafted to see the change in STS parameters near the step edge defect with respect to the lower terrace and the upper terrace. Following conclusions can be drawn from the table.
(i) the attenuation in the onset energy for the upper terrace is higher than the lower terrace (Tab. 2, *first row*),
(ii) major of the processes ($\triangle$) are taking place within 3 nm from the defect for either terrace (Fig. 13-*second column*) with irregular distribution (Tab. 2, *second row*), (iii) on average, a three-fold increased in the electron population is seen in the lower terrace (Tab. 2, *last row*).

4.3. Two Dimensional Confinement

In this case, we evaluate and examine the surface state of the electron in a confined space having step edges as a 1-dimensional defect similar to Sec. 4.2. The presence of a step edge offers a step potential to the electron. Therefore, the STS spectra recorded in this case encompass two effects to analyze, (i) a box-liked confined structure and (ii) a step edge defect. To analyze both cases, the following methodology is employed. For the former case, the STS spectra are taken outside the confinement, i.e., on the terrace (Fig. 14(a)), so as to decouple the confinement effect in the electron LDOS. And for the later, the step edge defect in confinement is compared with the earlier case of the step edge defect (Sec. 4.2 Pg. 21).

The STM image of the confinement is a parallelogram-shaped pit with dimensions of ((25.0 $\times$ 37.5) nm^2 $\pm$ 0.1 nm^2) and an angle of 120° (Fig. 14(a)). The box-like confined structure has a step height of 0.20 nm. The STS spectra were recorded diagonally to one of the longer step edges. In the confinement results, many peaks become more apparent that were not evident in the earlier 1-dimensional defects. Specifically, this study compares one point in confinement to one point on the terrace, equidistant from the defect line. On this basis, L1 (confined space) is compared with L8 (on the terrace), L2 with L7, L3 with L6, and L4 with L5 (Fig. 14(a) and Fig. 15). Further, each STS spectra contains *yellow, green* and *red* dotted vertical lines, transferring the dI/dV curve. This line indicates the occurrence of peaks in the confinement and on the terrace.

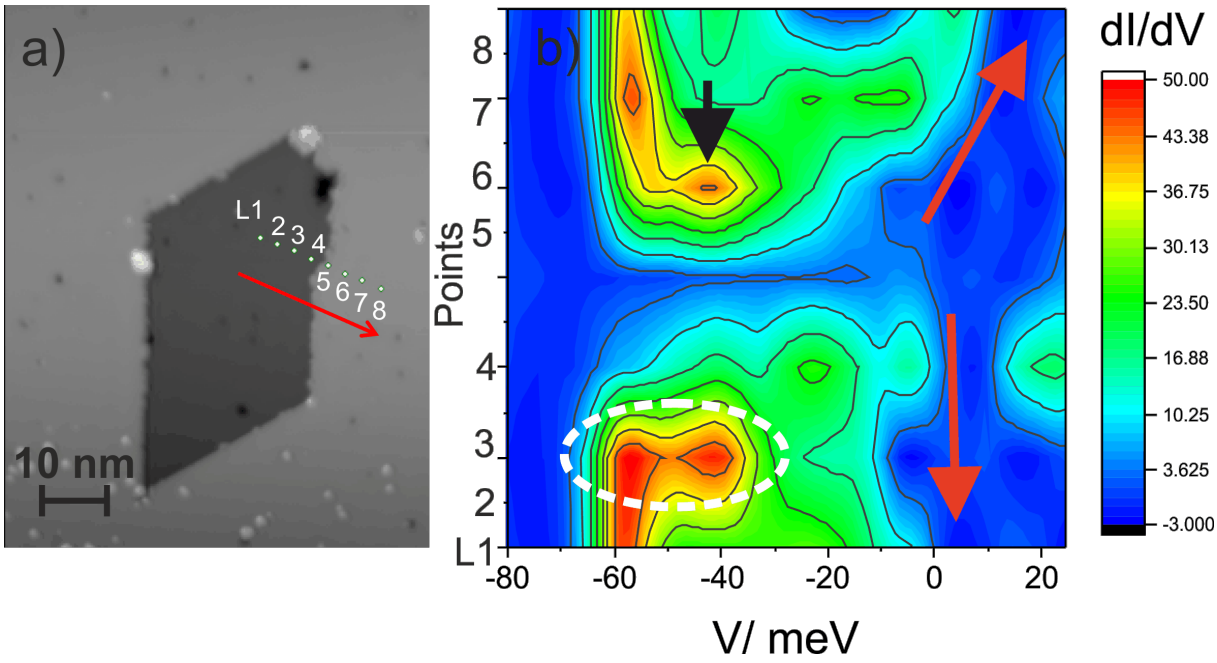

Figure 14: Effect of 1-dimensional defect on the LDOS in confinement. (a) STM image of the confined space. Tunneling parameters: -0.2 V, 1 nA, at 5 K. (b) A contour plot of the STS spectra. The white *ellipsoidal* dotted mark indicates the occurrence of two peaks and the black arrow marked the occurrence of the second peak. The big red arrows indicate the dispersion of the dI/dV vs V in the confinement vs on the terrace.

4.3.1. L1 - L8: Change in Electron Population

Here both L1 and L8 are ∼10.2 nm away from the step edge defect (Fig. 14(a)). The STS spectrum (dI/dV) for L1 has shown an onset peak followed by a higher peak at higher energy (Fig. 15(a-i)). Then, the dI/dV gradually decreases till V=-30 meV, stays constant till V=-8 meV. Finally dI/dV drops to zero near the Fermi energy. A step-like rise is seen near the Fermi energy. This indicates the opening of the inelastic tunneling channel (Fig. 15(a)-*yellow arrow*). A detailed analysis of the inelastic processes will be discussed in the next part of this case (P. 27). Whereas, in L8 (Fig. 15(a-ii)), the first rise in the onset peak is at -60 meV followed by a gradual decrease, and then, one more peak occurred around -40 meV. The STS parameters obtained for L1; the onset energy occurred at (-68 ± 1) meV, the broadening is (16 ± 1) meV, and the intensity is (354 ± 2) arb. unit. Whereas in L8, the onset energy is (-62 ± 1) meV, the broadening is (11 ± 1) meV, and the intensity is (55 ± 1) arb. unit. A more than six-fold increase in electron population is seen in the confinement.

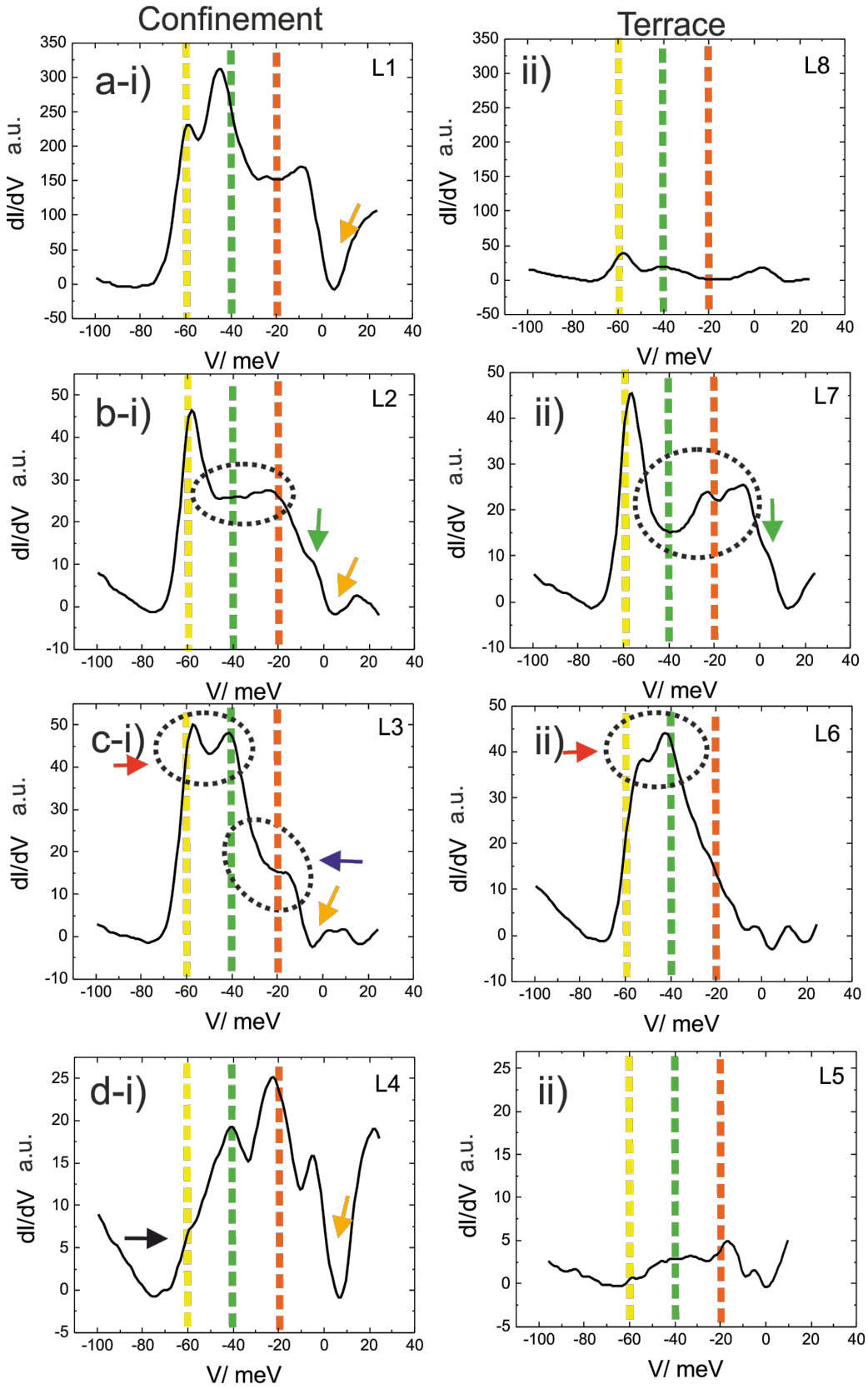

Figure 15: STS spectra in 2D confinement and on the terrace. (a) Each window contains the respective STS spectrum. Different colours arrows are marked to indicate the emergence of peaks (electronic surface state) and tri-colour dotted lines signify the pattern observed across all the STS spectra.

4.3.2. L2 - L7: Non-Perturbative Environment in Confined Spaces

L2, taken at ∼7.3 nm from the step edge in the confinement, exhibits a remarkable difference when compared to the same dI/dV obtained on the upper terrace (L7) at ∼6.4 nm (Fig. 15(b)). In confinement, L2 has a first rise at (-63 ± 1) meV, with broadening (△) of (12 ± 1) meV, and an intensity (**I**) of (67 ± 3) arb. unit has no other peaks at higher energies. Whereas for L7, the onset energy is (-62 ± 1) meV, the broadening is (11 ± 3) meV and the intensity is (58 ± 1) arb. unit (Fig. 15-b(i,ii)).

The physical interpretation of the dI/dV spectrum in confinement studies is subjected to the geometry of the system. In L2, after the surface state onset, a constant dI/dV is observed after V=-50 meV (Fig. 15-b(i), *dotted ellipsoid*). Further, a peak masked by the decreasing dI/dV spectrum (*green arrow*) occurred near the Fermi energy. On the terrace (L7), the onset peak is followed by a cusp at V=-30 meV and then a couple of peaks occurred at higher energies (Fig. 15-b(ii)-*marked ellipsoid*). On the other hand, the L2 spectrum displays non-perturbative behavior with higher energies. A possible explanation for this phenomenon is the conservation of momentum. Electrons with momentum perpendicular to the surface preferentially tunnel. However, with increasing energy, the in-plane momentum ($k_{\|}$) increases. This results in the suppression of the tunneling conductance and causes a decrease in signal [**?**]. However, an electron in the confinement experiences lateral trapping. This results in a shallow potential well [**?**]. The geometry of the confined structure raises the energy eigenstate, which leads to an increase in in-plane momentum. Therefore, after -50 meV a constant dI/dV is observed (Fig. 14-b(i), *marked ellipsoid*).

One more observation seen in the confined structure is the occurrence of the step-like function near the Fermi energy. Osterhage *et. al.* briefly discussed the similar spectroscopic signature exhibited in Be(0001) at the Fermi energy. This step-like function near the Fermi energy is symmetrical [**?**]. This feature in the STS indicates the opening of the additional tunneling channels that are connected to the inelastic electron-electron scattering and phonon coupling (Fig. 15-*left column yellow arrow*). This inelastic tunneling channel becomes viable only at higher energy, on top of the elastic tunneling [**?**].

4.3.3. L3 - L6: Spatio - Temporal Resolution in Confined Space

In this case, L3 in the confinement is at ∼4.4 nm and L6 on the terrace is at ∼3.5 nm away from the step edge defect (Fig 14(a)). The STS parameters obtained for L3; the onset energy occurred at (-62 ± 1) meV, the broadening is (14 ± 1) meV, and the intensity (**I**)

is (73 ± 4) arb. unit. And for L6; the onset energy is (-60 ± 1) meV, the broadening is (13 ± 1) meV, and the intensity is (56 ± 1) arb. unit. On the comparative ground, a 27% increase in the electron population is exhibited by the confinement.

The feature exhibited by both L3 and L6 - STS spectrum contains multiple peaks (Fig 15(c)). In the confinement, the onset peak is higher in intensity than the second occurring peak. Whereas in L6, the onset peak is lesser in amplitude than the second occurring peak. This shift in the intensity between the first peak and the second peak is solely attributed to the confinement-like effect. Moreover, in confinement, the quantization of the electron leads to the occurrence of minimal 2 or maximum of 4 peaks. On the terrace, a single onset peak exists in the absence of the defect (Fig. 5c(ii)). However in the presence of the defect, multiple peaks are observed in our work (Fig. 19(a,b)-*red arrow* Pg. 36).

In the contour plot (Fig. 14(b)), at L3 two dominant red dots (peaks) are encircled with *white dotted ellipsoid*. Whereas in L6, the only second peak is dominant (*encircled and marked with red arrow*). The intensity of the L6 is lesser than the L3 STS spectrum. So from the contour plot, two conclusions can be incurred; (i) The occurrence of events (two peaks in the STS spectrum) in confinement are bound by spatial limits. Further, the intensity of the second peak does not mask the onset peak, unlike the STS spectrum on the terrace. And (ii) the intensity of STS spectra is visibly higher in confinement.

The third observation is regarding the conservation of mass within the confinement. The entity that is restricted by the geometry of the system is the electron population. Unlike open space, an electron present in the confined space experiences a step-potential to bypass the spatially bound space, and on an equal footing exhibits the quantized energy states as per the geometry of the confined space. This restricts the electron diffusing from the open surface to pass into the confined space. A similar scenario is seen in the current case. A short comparison is made among the 1-dimensional defects to emphasize and reiterate our observed results. The Table 3 presents the STS parameter evaluated at (4.2 ± 0.5) nm from the 1-dimensional defects in the lower terrace.

Table 3: Comparison of the STS Parameters.

STS surface	E/meV	△/meV	**I**/ arb. unit.
L3 - Confinement	-62 ± 1	14 ± 1	72 ± 4
Slip Plane Disl.	-66 ± 1	26 ± 5	233 ± 7
Step Edge Defect	-58 ± 1	29 ± 1	342 ± 3

In Table 3, the electron population in the confinement is ≈ 70% lesser than the slip plane

dislocation and ≈ 80% lesser than the step edge defect. On the whole, comparatively lesser than the two earlier mentioned 1-dimensional defects. This assumption of conservation of mass (electron) in confinement is plausibly acceptable.

4.3.4. L4 - L5: Energy Eigenstate and Loss of Signal

The STS spectra are taken next to the defect, i.e., L4 at 1.65 nm in the confinement and L5 at 0.95 nm on the terrace. Compared to the previous two cases, the STS spectra obtained here are trivial. The only observable entity is present in the L4 STS spectrum, i.e., the peaks in the confinement were well resolved and separated. The first peak occurred at -60 meV (onset energy), the second at -40 meV, the third at -20 meV, and the fourth peak occurred around the Fermi energy (Fig. 15 d(i)). A total of four peaks occurred in the confinement with the onset peak is being masked (Fig. 15d(i)-*black arrow*) by the second peak. Moreover, a step-like function is seen near the Fermi energy. Further, the third peak is higher in intensity than other peaks in L4. This is not seen in earlier nor in the latter cases to come. Whereas in the contour plot, all the peaks in L4 have exhibited low intensity with only the third peak has managed to exhibit an effect (Fig. 14(b)). Further, the appearance of the fourth peak before the Fermi energy is solely attributed to the presence of the confinement. As none of the cases discussed earlier has shown this feature. Secondly, the electron LDOS near the line defect is dominated by the electron-defect scattering, followed by elastic electron and phonon coupling, and near-zero by inelastic processes.
The STS parameter evaluated for L4; the onset energy is (-58 ± 1) meV, the broadening is (36 ± 1) meV, and the intensity is (48 ± 5) arb. unit. In L5; the onset energy is (-47 ± 1) meV, the broadening is (49 ± 2) meV, and the intensity is (15 ± 6) arb. unit. The electron population is relatively higher in confinement but lower than the earlier mentioned values.

For the L5 STS spectrum on the terrace, the surface state electrons are more perturbed. None of the peaks are distinguishable. Only a peak near the Fermi energy is visible.

4.4. Comparative Studies for 1-Dimensional Defect

The closing remarks for the 1-dimensional defects on Ag(111) are done on the qualitative ground. The STS points are compared on a spatial basis. The lower terrace of the slip plane dislocation (Sec. 4.1) is compared with lower terrace of the step edge defect (Sec. 4.2), and with the inside of the 2-D confinement (Sec. 4.3), and similarly for the upper terrace. Since the defects discussed earlier have different topography, the processes that occurred

at the defect site vary accordingly. The bulk-surface mixing, electron-defect scattering, and elastic to inelastic contribution towards the electron-and-phonon coupling and lateral relaxation (oscillation) of the electron all varied as per the defect. A cumulative graph of all the STS parameters is presented in Fig. 16. In Fig. 16(a-b), the Gaussian fit was applied over the onset energy and broadening of the onset energy. Whereas in Fig. 16(c), sine wave function fits well. However, for step edge defects, the points are widespread and no functional systems fit well on the set of points.

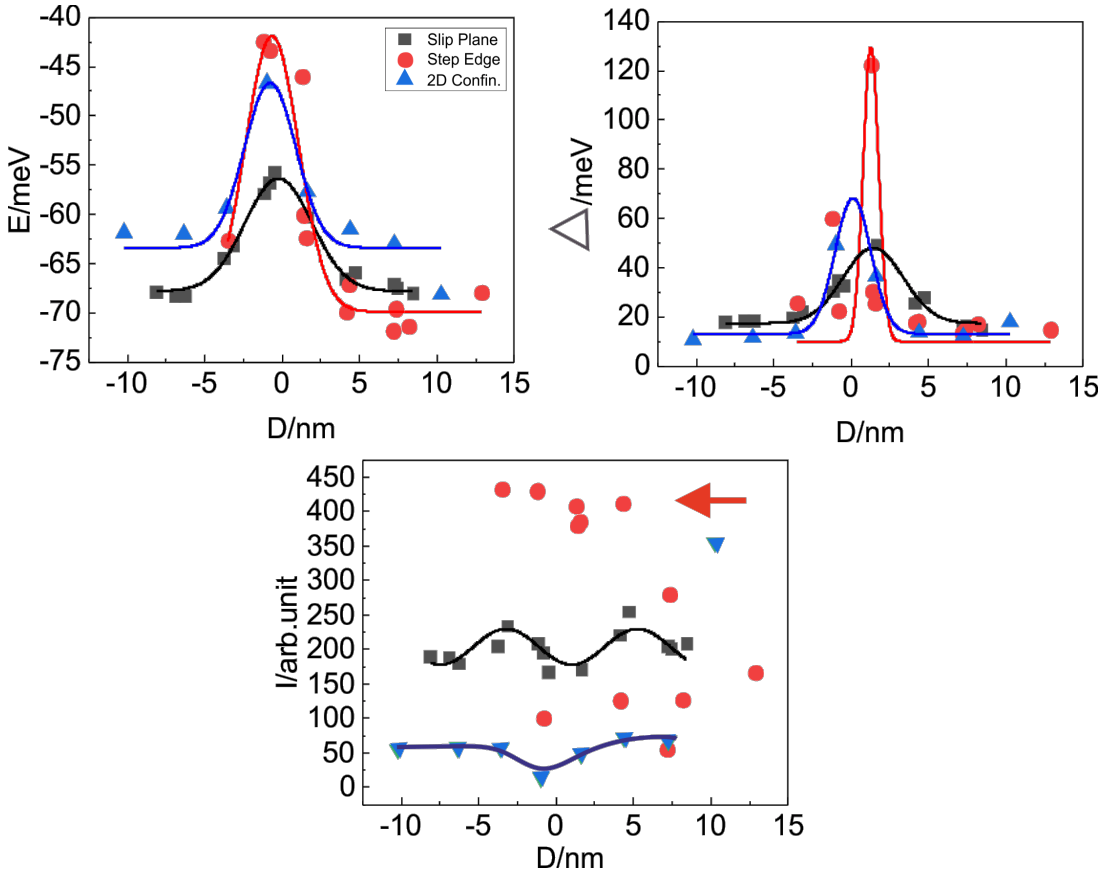

Figure 16: Comparative graph for the different defects. (a) Onset energy (E/meV) vs distance (D/nm). The fit represents the possible trend to see in onset energy. In (b) broadening of the onset energy (△/meV) vs distance (D/nm), and (c) intensity of the electron population (**I**/arb unit). In (b) almost all the broadening processes in each defect fall within the same range. Only one point in step edge defect was at a higher value and in (c), the arrows mark the electron population of each defect.

Following conclusions can be drawn from the discussion so far;

- A decrease of the onset energy over a distance of (2.5 ± 0.2) nm in the step edge is -65 meV to -35 meV, slip plane is -65 meV to -50 meV, and in confinement is -61 meV to -47 meV (Fig. 16(a)). The maximum change occurs for the step edge defect.

- The broadening of the onset energy for all the defects has shown a similar pattern and change in values to the 1-dimensional defect (Fig. 16(b)).
- The electron population has become the prominent STS parameter that plausibly categorizes the effect induced by the defect. The change in structural topography directly affects the electron population. Moreover, confinement has the lowest electron population. This also supports our conjecture of conservation of mass (Fig. 16(c)).

Section II

The current section deals with the surface state electron near the 1-dimensional defect induced by the NaCl(100) island on Ag(111) substrate. As the direction of the STS recording changes and the island orientation varies as per the adsorption site, these allow categorizing the results into four cases,

1. The surface state of the electron near the edge of the NaCl(100) island is grown over the bare Ag(111) substrate.

2. The effect of the non-polar edge [001] of the NaCl(100) and the step edge of the Ag(111) on the LDOS.

3. The effect of the vertex and the salt edges of the NaCl(100) on the LDOS. An example of lateral confinement of the electron.

4. The second case for analyzing the vertex effect, partially independent of the salt edges on the LDOS. Further, the effect of the polar edge of the NaCl$\langle 011 \rangle$ on the LDOS.

4.5. NaCl(100) island on Ag(111)

In this case, we analyze the surface state of the electron near a rectangular NaCl(100) island. The studied island has a dimension of ((20 nm $\times$ 15 nm) $\pm$ 0.1 nm) on Ag(111). The NaCl(100) island has a lattice mismatch of 2.7% with Ag(111). This results in the atomic orientation of ions (Na^+ and Cl^-) in NaCl(100) with a (1.5 $\pm$ 0.5)% deviation from the bulk in $\langle 112 \rangle$ direction and perfectly fits well in $\langle 110 \rangle$ direction [19]. The change induces strain on the Ag(111) and affects the surface state up to $\sim$15 nm from the island [19].

STS spectra are recorded across the island along the long axis in the direction of the red arrow from **A** to **B** with 50 data points in total (Fig. 17). The first STS spectrum is recorded $\sim$30 nm away from the salt edge on side **A**. The onset energy is (-69 $\pm$ 1) meV, the broadening ($\triangle$) is (18 $\pm$ 4) meV, and the intensity of the electron population (**I**) is (3 $\pm$ 1) arb. unit. Similar results are reported in [7,14]. Further, the broadening ($\triangle$) = (18 $\pm$ 4) meV gives an electron lifetime in between $\sim$135 fs (upper limit) and $\sim$80 fs (lower limit) using the equation-10 (Pg.12). And at the interface on either side, the onset energy is (-59 $\pm$ 2) meV, the broadening is (16 $\pm$ 2) meV, and the intensity is (27 $\pm$ 10) arb. unit. It gives the lifetime $\sim$(98 $\pm$ 12) fs.

Next, a short comparison is done between side **A** and side **B** on a spatial basis to analyze the difference in the LDOS. The farthest STS point on the side **B** is 20 nm away from the defect, therefore an STS with equal distance is considered on side **A**. On side **A** at 20 nm

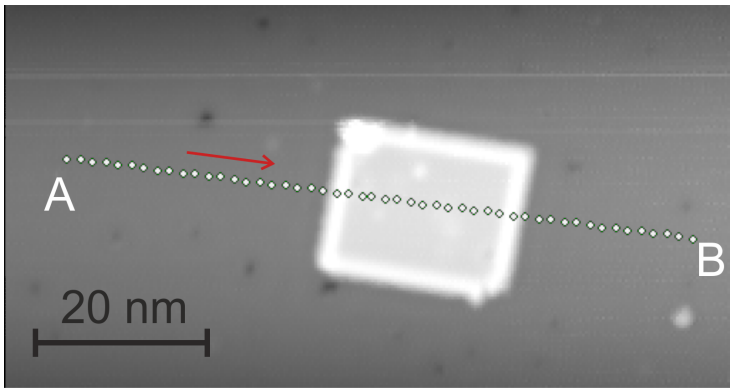

Figure 17: STM image of NaCl(100) island on bare Ag(111) surface. The white dots represent measurements of STS spectra. The spectra recorded from A to B are marked with a red arrow. The height of the island is 0.245 nm at -0.2 V. Tunneling parameters: -0.2 V, 0.19 nA, and 5 K.

from the salt edge, the onset energy is (-69 ± 1) meV, the broadening is (9 ± 1) meV, and the intensity is (45 ± 2) arb. unit. The calculated lifetime on side **A** is (55 ± 7) fs. Whereas on the right side, the onset energy is (-68 ± 3) meV, the broadening is (12 ± 3) meV, and the intensity is (44 ± 4) arb. unit. The broadening on the side **B** gives the lifetime = (74 ± 19) fs. A 34% more lifetime is recorded on side **B**. Though, the lower limit (=55 fs) of the lifetime on side **B** is equal to the median (=55 fs) of the lifetime on side **A**. This uncertainty in calculation exists due to instrumentation limits.

The presence of a salt island affects the LDOS up to ∼20 nm on either side of the island in our case (Fig. 18). However, the major shift in the STS parameters occurred at 10 nm away from the island. Now, dividing this 10 nm spatial length into two halves, the first 5 nm bring about a 2 meV change in the onset energy, and the remaining 5 nm close to the island brings ∼8 meV change. An exponential-like rise is seen in the onset energy near the island. And for the other STS parameters, an increase of (8 ± 2) meV in the broadening and a decrease of (28 ± 3) arb. unit for the intensity is seen in the range of 10 nm from the island. On the whole, the major processes are occurring under 5 nm from the island.

- Comparison of NaCl(100) Island with Slip Plane Dislocation

A step edge of NaCl(100) is symmetrically identical in topography to a slip plane dislocation (Sec. 4.1 Pg. 18). However, a step edge of the slip plane has dipole characteristics. NaCl(100), on the other hand, is composed out of alternating Na^+ and Cl^- ions of a bilayer height (Fig. 2(d-e) Pg. 6). These differences in the electronic structure explain the observed LDOS changes along the path from the substrate to adsorbate. The change in the onset energy over the range of 10 nm in NaCl(100) towards the edge is (10 ± 1) meV

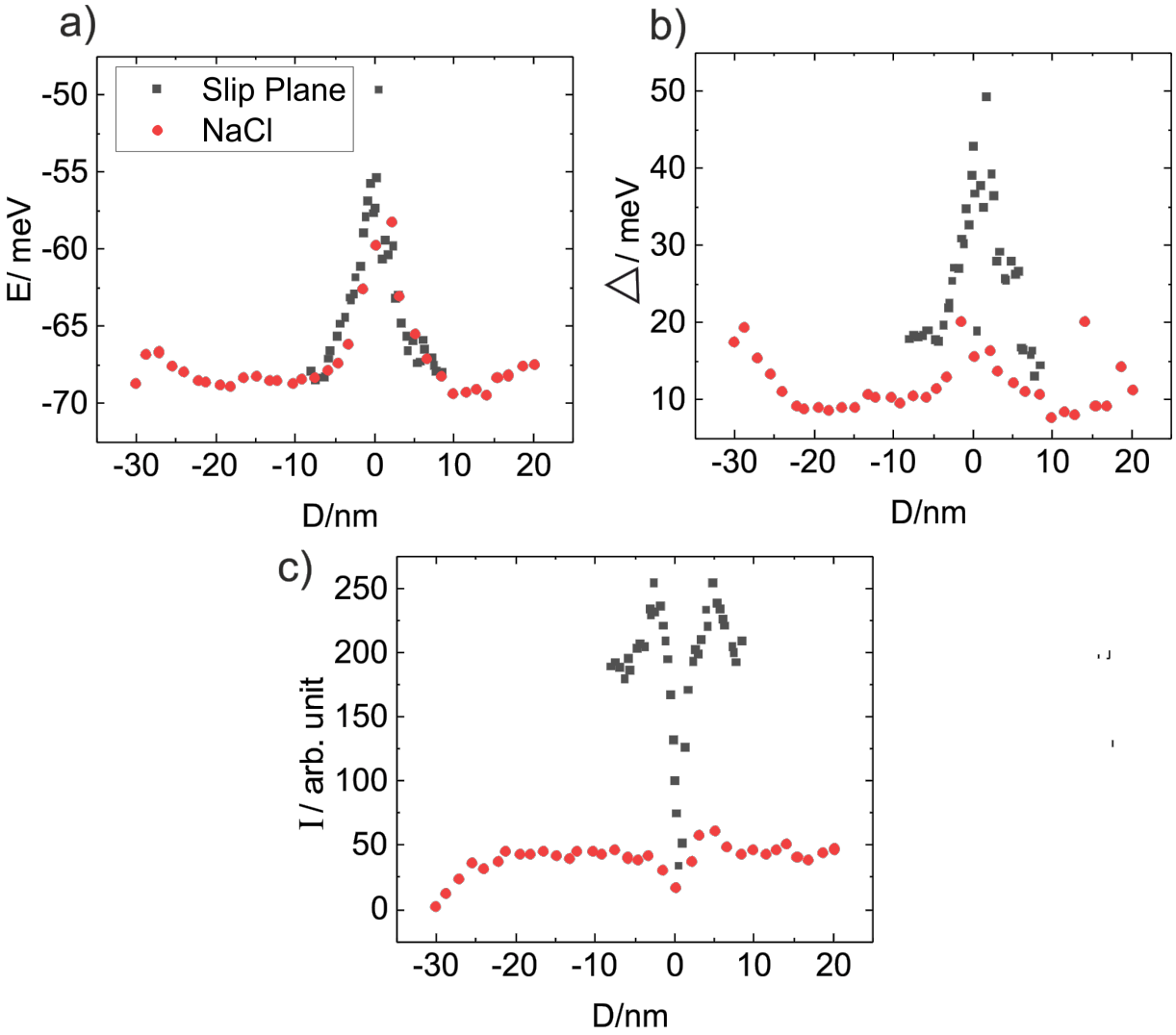

Figure 18: A comparative graph between NaCl(100)-Ag(111) substrate vs slip plane dislocation. (a) Onset energy (E/meV) vs distance (D/nm), (b) broadening (△/meV) vs distance (D/nm), and (c) intensity of the electron population (**I**/arb. unit) vs distance (D/nm).

and (18 ± 1) meV in the slip plane dislocation (Fig. 18(a). Whereas, the change in the broadening is (8 ± 1) meV in NaCl(100) and (32 ± 2) meV in the slip plane dislocation (Fig. 18(b). And for the electron population, more than 7 times reduction is seen near the NaCl(100) island compared to the slip plane dislocation (Fig. 18(c)).

The physical interpretation of the change in LDOS near the NaCl(100) island is the presence of a full crystal NaCl-bandgap at 8.9 eV [6, 19]. For an electron near the island, this bandgap acts as a step potential. Further, the charge distribution around the salt edges of the NaCl(100) island possibly exhibits an influence on the LDOS. A seven-fold drop in electron population and a three-fold drop in broadening near the island compared to

the slip plane dislocation. In brief, NaCl(100) influences the surface state of the electron similar to the slip plane dislocation but less pronounced.

4.6. 2-D Structured Barrier: Edge Effect on Electron LDOS

In this part, NaCl(100) island adsorbed at the step edge of the Ag(111) substrate in a triangular shape. This leads to the polar edge [011] of the NaCl(100) exposed to the surface state electrons [6]. The STS spectra are recorded across the [001]-edge of the NaCl(100) and continued over the island followed by the upper terrace of the Ag(111) substrate (Fig. 19(a)). A 2-dimensional structured barrier or confined space is formed by the step edges of the NaCl(100) and Ag(111) substrate. This topography partly facilitates the principle of 2D confinement near the step edges. Though with the exception that the opposite to the step edges exist an open system. It affects the formation of the standing waves due to non-confinement. It makes our first observation in deciphering the change in electron LDOS near the step edges. Following, the STS spectra recorded opposite to the polar edge [011] on the upper terrace have distinctly affected the LDOS. The exhibited nature by the polar edge on the upper terrace became our second observation in this case study. Therefore, to analyze the change in STS spectra across the system, we will treat each point on an individual basis. Here, a brief table for the STS data points measured from the edge of the NaCl(100) and Ag(111) is given in Tab. 4.

The STS spectra are recorded on the lower terrace (L1 and L2 - STS spectra), at the interfaces between NaCl[001] and lower terrace of the Ag(111) (L3-STS spectrum) as well as between NaCl[011] and the upper terrace (L4-STS spectrum), and the last one on the upper terrace of the Ag(111) (L5-STS spectrum) (Fig. 19(a), Tab. 4). The L1 (STS spectrum) has an onset peak followed by a gradual drop to V = -53.7 meV. Later, maintained a constant dI/dV till V = -41.4 meV. And finally, a smaller intensity peak occurred at V = -14.8 meV and then, dI/dV goes to zero near the Fermi energy (Fig. 19(b)). A step-like rise is seen around the Fermi energy. This indicates an opening of the inelastic electron tunneling and phonon coupling [**?**]. Further, the electron population is higher than the earlier discussed case of simple NaCl(100) on bare surface (Sec. 4.5 Pg. 32). The possible explanation for the higher electron population is the presence of Ag(111) step edge. This leads to higher electron density in the lower terrace and affects the LDOS up to ∼10 nm. A five-fold change is seen in electron population in the presence of the Ag(111) step edge compared to Sec. 4.5. The effect from the step edge on the electron population in the lower terrace is briefly discussed in Sec. 4.2 (Pg. 21). In total, three peaks emerged for the L1 with a step-like function at the Fermi energy.

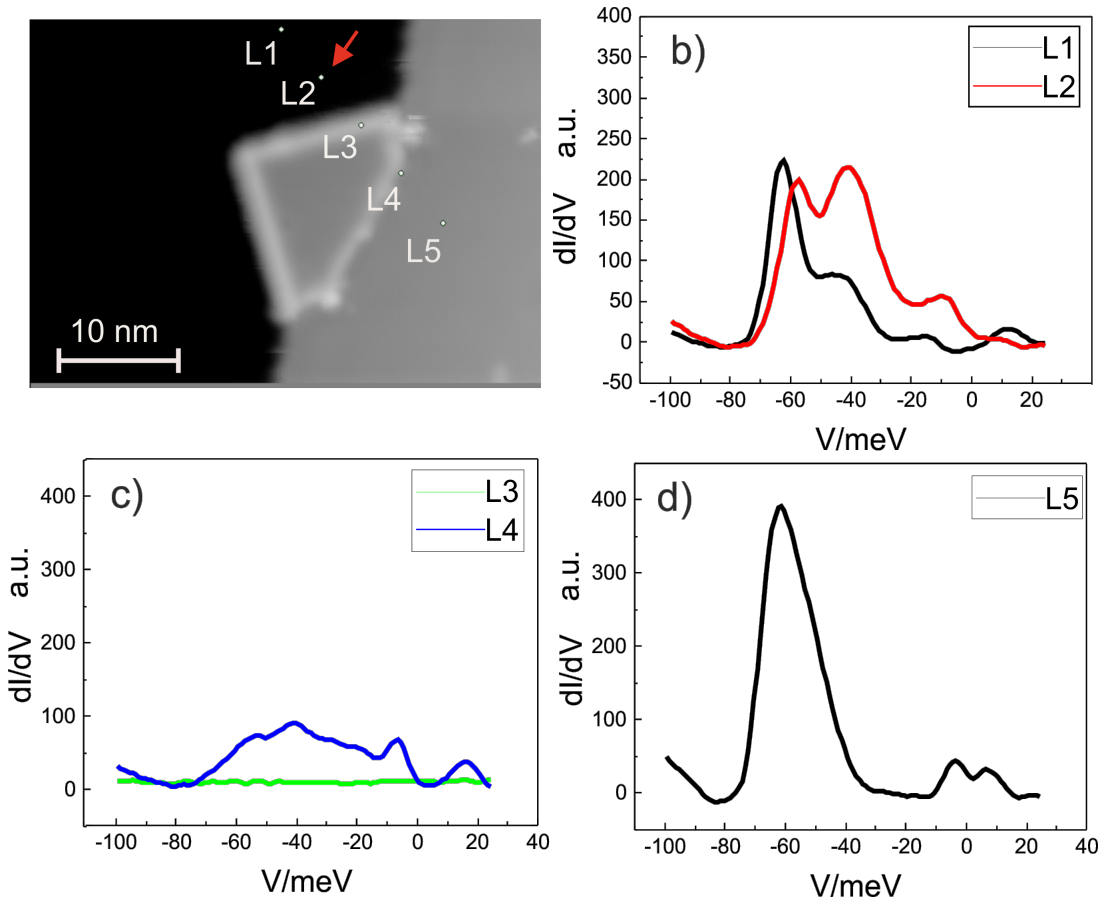

Figure 19: Step edges effect on the electron LDOS in a 2-D structured barrier. (a) An STM image of NaCl(100) adsorbed at the step edge of Ag(111). Tunneling parameter: -0.3 V, 0.2 nA, 5 K, and V_{mod}=30/7 V. (b) STS spectra of L1 and L2 on Ag(111)-lower terrace, (c) STS spectra of L3 and L4 at the lower and upper interfaces, and (d) STS spectrum of L5 on the upper terrace of Ag(111). The height of the island is 0.245 nm at -0.3 V.

Table 4: The STS parameters were resolved spatially from the NaCl(100) and Ag(111) substrates.

STS	D_{NaCl}/nm	D_{Ag}/nm	E/meV	△/meV	**I**/arb. unit
L1	7.9	9.9	-62 ± 1	15 ± 1	279 ± 14
L2	2.6	6.3	-63 ± 1	20 ± 1	296 ± 23
L3	0	0	33 ± 1	15 ± 2	25 ± 17
L4	3.2	3.2	-63 ± 1	27 ± 3	155± 15
L5	5.6	5.6	-67 ± 1	12 ± 2	539 ± 19

In L2 (Fig. 19(a) - *red arrow*), total three peaks occurred. The first onset peak at V = -58.4 meV, the second peak at V = -40.4 meV, and the last one at V = -9.4 meV. Secondly,

a step-like rise is not prominent at the Fermi energy in this STS spectrum. However, a similar spectrum is recorded in 2D confinement (Sec.4.3 Pg. 24 Fig. 14(c-i)). Referring to the Fig. 14(c-i) in 2D confinement, there the onset peak occurred at V = -57.4 meV, the second occurred at V = -42.4 meV, and the last one occurred at V = -15.5 meV. Significant observations are the occurrence of the second and the third peak in both systems around the same bias voltage. This suggests that certain electronic structures are found only near the spatially constrained and bound environment near the step edges.

The L3 is recorded at the interface, exemplifying the idea of bulk-surface mixing underneath the adsorbate (Fig. 19(c)). The precipitative nature of the electron at the interface comes due to the bandgap and lattice mismatch. This leads to electron-electron scattering leading into the bulk and the loss of momentum is then compensated by the electron-defect scattering. Further, a drop in electron population is seen at the interface. Referring to Table 4 (*third row*), ≈90% drop in electron population is seen at the interface compared to previous STS point (L2) over a distance of ∼2.6 nm.

Next, L4 and L5 - STS spectra are taken opposite to the polar edge $[0\bar{1}\bar{1}]$ of the NaCl(100) and on the upper terrace of the Ag(111) substrate. The characteristic change in the STS parameters occurred especially in the intensity of the electron population. Due to the polar edge of the NaCl(100), it creates a charge zone over the upper part of the step edge in Ag(111). This repels the negatively charged electron away from the polar edge. A detailed discussion is done in the last case of this Section II in Sec. 4.8.2 (Pg. 44).

4.7. Lateral Confinement of the Surface State Electron

The STS spectra are recorded in $\langle 0\bar{1}0\rangle$ direction, parallel to the non-polar edge-$[0\bar{1}0]$ of the NaCl(100). The topography is similar to the earlier case (Sec. 4.6 Fig. 19(a) Pg. 36). The only difference is the direction of the STS spectra recorded (Fig. 20 (*STM image*)). This case allows to study of the purely geometric effect from the island's edges, i.e., $[0\bar{1}0]$ and [001], and the vertex. The STS is recorded from a 6 nm (Fig. 20 (*scale on the right side of the STM image*)) laterally above the island (long axis of the image), measured from a vertex. A total of 90 STS points are recorded. Four different regions are identified that has displayed characteristics changes in STS spectra (Fig. 20 - *marked with arrows*).

The region of the STS spectrum in the range between 6 nm and 3 nm (Fig. 20 - *scale on the right side of the STM image*), away from the vertex is considered as region-I (Fig. 20-*arrow*-1). The onset energy is (-64 ± 1) meV, the broadening (△) is (10 ± 1) meV, and

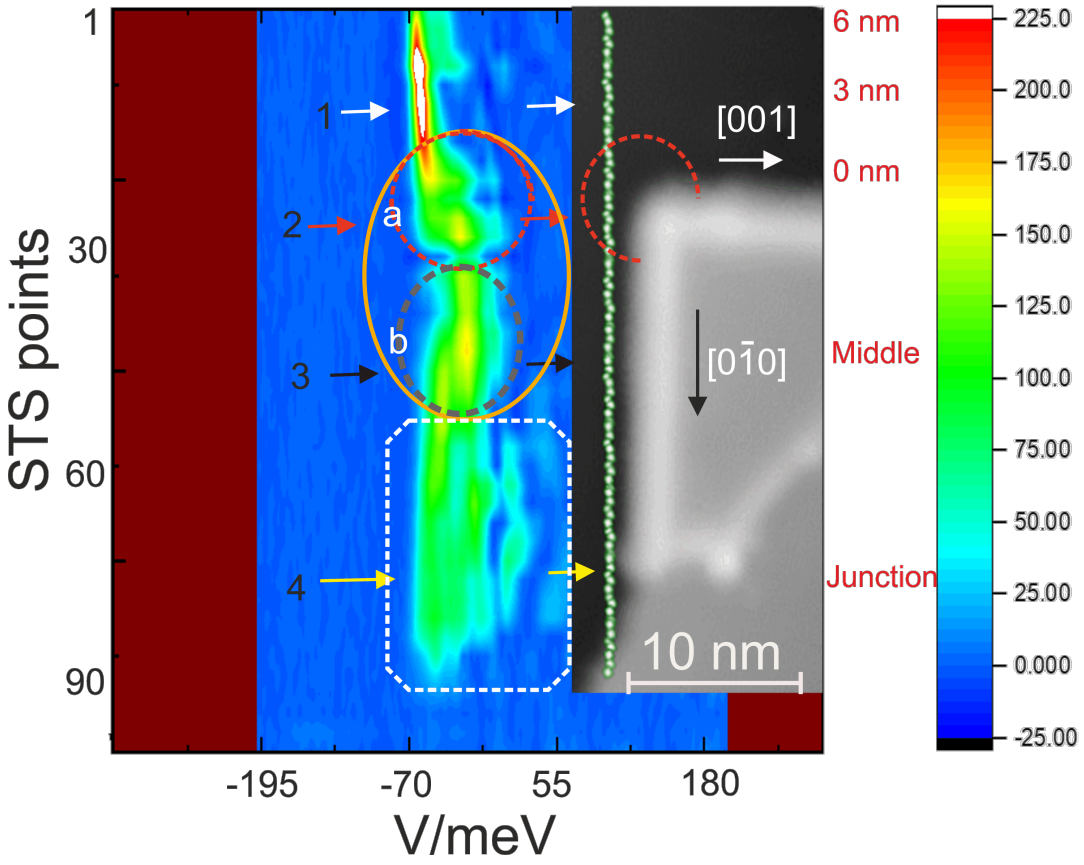

Figure 20: LDOS near the vertex and the non-polar edges of the NaCl(100). The contour plot comprehensively displays the LDOS as per the topography. An STM image is presented on the right side of the contour plot along with a distance scale (red colour). The STS is recorded in $\langle 0\bar{1}0 \rangle$ direction (white dot). On the right, the scale bar of the dI/dV a.u. Arrows are marked to highlight the changes seen in the contour plot. Tunneling parameters: -0.3 V, 0.2 nA, 5 K, and $V_{mod} = 30/7\ V$.

the intensity of the electron population (**I**) is (294 ± 60) arb. unit. The calculated lifetime with the given broadening is (61 ± 4) fs. A dominant bright streak of onset peak (*opposite to arrow*-1) is seen in the contour plot.

Next, the STS spectra are recorded next to the vertex of the NaCl(100) at ∼1.65 nm (Fig. 20 - *arrow marked*-2 and *red dotted circle*-**a**) is referred as region-II. The effect from the vertex is pronounced. An inward bend in the STS spectra is seen in the contour plot. This displays a positive shift in the onset energy towards the Fermi energy in the presence of the vertex. Moreover, this shift in the onset energy begins at ∼2 nm laterally above the vertex, reaches its maximum at 1.65 nm (opposite to the vertex), and extends down to 2.66 nm in the direction of the non-polar edge-$[0\bar{1}0]$ of the NaCl(100). It can be inferred that the electronic influence of the vertex is extended over a circular region (Fig. 20

STM image - *red dotted 3-fourths of the circle*). Though the STS took parallel to the non-polar edge has an effect contributed from the vertex. This creates an ellipsoid-like spread of the LDOS (Fig. 20 - *black dotted ellipsoid marked with*-**b**). All-together, a long ellipse (Fig. 20 - *organ colour*) from above the vertex and extends in the direction of the non-polar edge $[0\bar{1}0]$ till the middle. Apart from the shift in the onset energy, a localized perturbation of the electron is seen near the vertex, i.e., shows a couple of minimal dI/dV peaks opposite to the vertex. For suppose, if an edge is considered as a straight line, then two-step edges ([001] and $[0\bar{1}0]$) intersection can be regarded as a common intersection point. Hence, a vertex has point-like characteristics, which makes the vertex behave like a point defect. This leads us to acknowledge the Friedel oscillation. However, a point defect is a dimensionless entity [**?**]. For that reason assuming a vertex as a point defect is only works as a first approximation. The localized perturbation near the vertex must be considered in order to describe the system completely. Finally, the STS parameters opposite to the vertex are; the onset energy is (-61 $\pm$ 1) meV, the broadening is (14 $\pm$ 2) meV, and the intensity is (283 $\pm$ 31) arb. unit. The calculated lifetime is (76 $\pm$ 3) fs. A $\sim$23% change in lifetime is introduced over a distance of 3 nm in $[0\bar{1}0]$ direction near the vertex.

Region III are the STS spectra taken in the middle of the non-polar edge -$[0\bar{1}0]$ of the NaCl(100) island (Fig. 20 - *arrow marked*-3). Here, the electron is laterally confined to the non-polar edge of the NaCl$[0\bar{1}0]$. At the middle of the non-polar edge, the onset energy is partially returned to its earlier value, i.e., shifted towards the surface state onset. At *arrow marked*-3, marks the boundary where the influence from the vertex has substantially ended. The onset peak is split into two peaks position at *arrow*-3 (Fig. 20 - *black dotted circle, marked with*-**b**). One onset peak is decaying and another is rising, rather than a smooth transition of the onset energy as seen near the vertex (Fig. 20 - *red dotted circle, marked with*-**a**). Secondly, the LDOS has minimal spread above and below the *arrow*-3. Unlike *arrow*-2, the onset peak was shifted inward and localized perturbation was dominant. To sum up, the total processes occurring parallel to the non-polar edge, firstly, a positive shift in the onset energy in the presence of the vertex and then, a negative shift in the onset energy along the non-polar edge. This leads to the occurrence of multiple maxima spread along the x-and y-directions. The electrons are thus confined independently in the two directions [15]. The STS parameters at *marked arrow*-**3** in Fig. 20 are; the onset energy is (-53 $\pm$ 2) meV, broadening is (31 $\pm$ 8) meV, and the electron population is (194 $\pm$ 15) arb. unt. To decouple the effect of vertex from the edge in LDOS, a short comparison is done here with the earlier case of NaCl(100) grown over the bare Ag(111) surface (Sec. 4.5 Pg. 32). At an equal distance from the salt edge in Sec. 4.5, the onset

energy is (-59 ± 1) meV, the broadening is (16 ± 2) meV, and the electron population is (17 ± 7) arb. unit. Therefore, in comparison, the presence of the vertex brings about a two-fold change in broadening and a relatively ten-fold change in electron population in the present case.

In region IV (Fig. 20 - *arrow marked*-4, **Junction**), the STS is taken at the junction. The topography of the junction is complex as it contains the end of the island, the upper and the lower terrace of the Ag(111) substrate. This all highly perturbs the electron LDOS. The contour plot (Fig. 20-*white dotted rectangle*) shows three low-intensity peaks in addition to a couple more peaks due to perturbation near the junction. The effect is spread out in x-and y-direction. Before moving towards why and how this phenomenon has occurred! The onset energy is (-59 ± 2) meV, the broadening is (34 ± 8) meV, and the intensity is (109 ± 51) arb. unit. In this region, a qualitative change is observed due to the complexity in structure. The onset energy increases alongside the broadening, which is not seen in our previous results. The electron population have dropped ∼45% with respect to (w.r.t) region III (*arrow-3*) and ∼60% w.r.t region II (*arrow-2*). Though, the presence of the Ag(111) step edge has not facilitated in the similar manner as it has done earlier in Sec. 4.6 (Fig. 19, L2-STS point), i.e., the presence of Ag(111) step edge has not increased the electron population. Here, the topography has governed the intensity of the electron population and the distance of the STS spectrum from the step edge of the Ag(111). In Sec. 4.6, the Ag(111) step edge is ≈10 nm away from the STS spectrum and the salt edge [001] is 2.3 nm away from the STS spectrum. Whereas, here, the STS spectrum is 1.65 nm away from the Ag(111) step edge and the salt edge. Since in the earlier case, the electron far away from the step edge defect behaves more like a surface state electron and less perturbed by the defect. And the second reason is the angle of confinement created by the [001] edge with the Ag(111) step edge (Sec. 4.6) and the $[0\bar{1}0]$ with the Ag(111) step edge (Sec. 4.6). The difference in angle between the two structured barriers is ≈12° more here. This changes the standing wave pattern formation. This can be a reason for the different LDOS.

4.8. Non-confinement Case

The STS spectrum is recorded across the NaCl(100) island in $\langle 0\bar{1}\bar{1}\rangle$ direction, bifurcating the island into two halves, creating a mirror image of the island and later, continued over the island and ends on the upper terrace of the Ag(111) (Fig. 21). The presence of the vertex and the polar edge exhibited a pronounced effect than the non-polar edge/s in the earlier cases (Sec. 4.5 and Sec. 4.7). Therefore, this case is divided into two sub-parts, (i) LDOS near the vertex and (ii) polar edge effect on the LDOS.

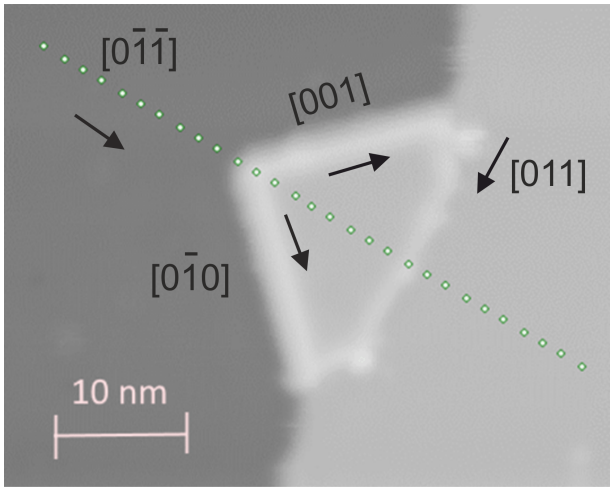

Figure 21: STM image of NaCl(100) island adsorbed at the step edge of the Ag(111). The STS spectra are recorded in $\langle 0\bar{1}\bar{1}\rangle$ direction to the NaCl(100) island. Tunneling parameters: -0.3 V, 0.2 nA, and 5 K.

4.8.1. LDOS near the Vertex

In this case and earlier (Sec. 4.7 P. 37), The STS recorded across the vertex has exhibited a positive shift in the onset energy, increase in the broadening, and first an increase and then a drop in electron density (Fig. 22). The STS trends observed here are different from all previous case studies (Sec. 4.5 and Sec. 4.7). This leads us to treat this topography separately and independently.

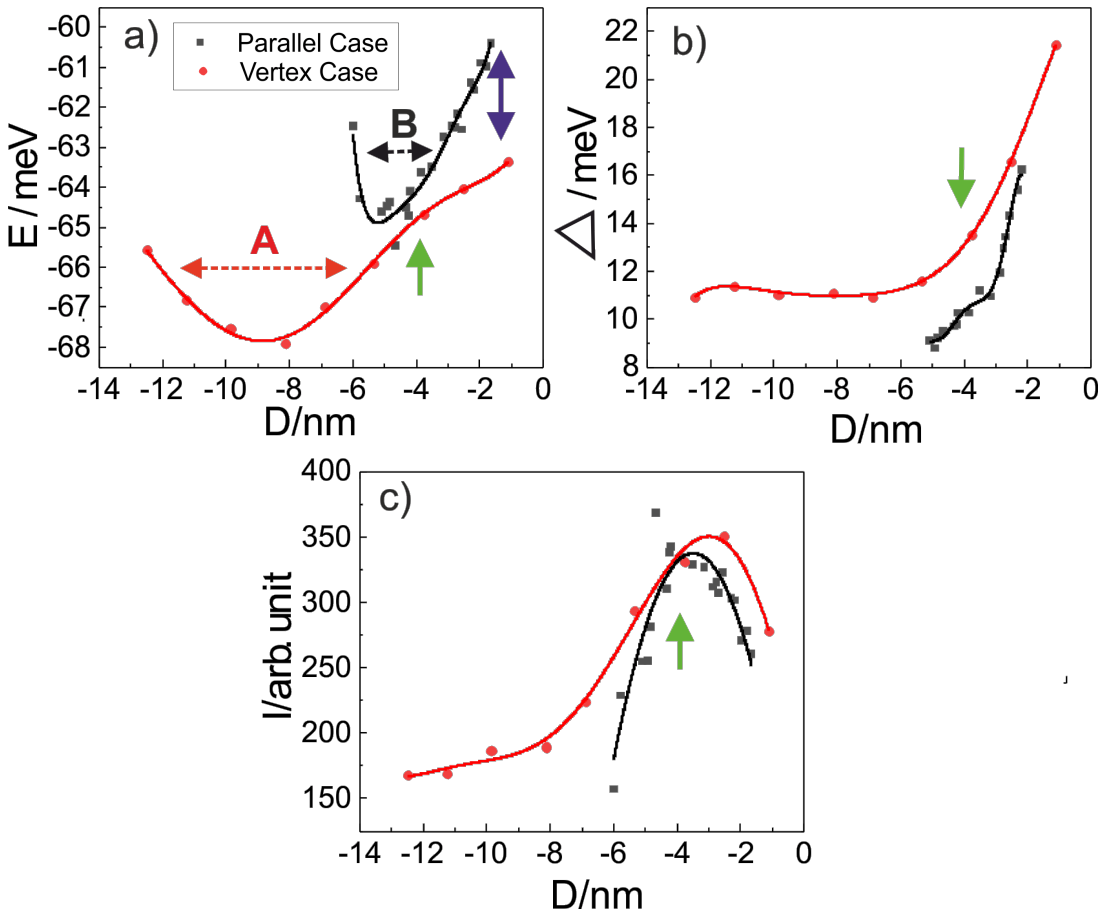

Figure 22: STS spectra recorded near the Vertex. A comparative graph of the STS parameter to exhibit the vertex effect on the electron LDOS. (a) Onset energy (E/meV) vs distance (D/nm). **A** and **B** indicates the latus rectum of the parabola. The purple arrow indicates the difference between the values due to a change in the topography. In (b) broadening (△/meV) vs distance (D/nm), and (c) electron population (**I**/nm) vs distance (D/nm). The lowest values in the x-axis indicate the furthest point from the vertex ($x = 0$). Parallel case means lateral confinement of the electron (Sec. 4.7). The green arrow indicates the change in STS trends occurred at the same spatial coordinate due to the presence of the vertex.

To decouple the influence of the vertex from the salt edges in the LDOS, a short comparison is done. The first case considered here is the simple NaCl(100) grown over the bare surface (Sec. 4.5 Fog. 17 Pg. 32). There the direction of the STS is orthogonal to the non-polar edge of the island. It decouples the vertex effect from the non-polar edge effect on the LDOS. The second case is the STS recorded in $\langle 0\bar{1}0 \rangle$ to the island (Sec. 4.7 Fig. 20 Pg. 38). The STS encompasses the effect exhibited by the vertex and $[0\bar{1}0]$ edge of the NaCl(100). The latter case is more meaningful in decoupling the vertex effect from the edge.

The closest STS spectra to the vertex are at ∼.165 nm in Sec. 4.7. In other words, all STS parameters fall within ∼.165 nm radius of the vertex will be discussed here. This ensures uniformity across the obtained results in each case. The STS parameters in this case from the vertex; the onset energy is (-63 ± 1) meV, the broadening (△) is (18 ± 4) meV, and the intensity (**I**) is (279 ± 76) arb. unit. In the island-grown on the bare Ag(111) surface (Sec. 4.5), the onset energy is (-63 ± 1) meV, the broadening is (13 ± 2) meV, and the intensity is (31 ± 5) arb. unit. And for the STS recorded parallel to the non-polar edge (Sec. 4.7); the onset energy is (-66 ± 1) meV, broadening is (16 ± 2) meV, and intensity is (244 ± 18). The following conclusion can be derived for the LDOS near the vertex,
(i) Vertex shifts the onset energy towards the Fermi energy by (2 ± 1) meV. In the presence of the non-polar edge of the NaCl(100) island shift the onset energy up to (4 ± 1) meV.
(ii) The broadening of the onset energy is substantially increased in the presence of vertex. Whereas, the broadening decreases near the salt edges as the electron is now laterally confined. This affects the lifetime of the electron. An electron near the non-polar edge and away from the vertex (Sec. 4.5) has a lifetime of ≈74 fs and in the presence of the vertex, it increases to ≈95 fs (Sec. 4.7). And lifetime near the vertex in the present case study, independent of the non-polar edges, further increases to ≈110 fs.
(iii) The density of the electrons is higher because of the vertex. The intensity drops substantially, in the absence of vertex or region away from the vertex. In the present case, a nine-fold increase in electron population is seen compared to the island-grown on the bare Ag(111) surface (Sec. 4.5). Whereas, the presence of an edge reduces the electron population up to ∼12% (Sec. 4.7). To further demonstrate 'how an edge and a vertex affect the LDOS?'. In Fig. 22, the STS parameters are plot for the vertex vs the lateral confinement of the electron of Sec. 4.7. In Fig. 22(a), the onset energy shows a saddle-or parabola-like structure when approaching near the vertex. The maximum shifts towards the Fermi energy occur in the presence of the edge (Fig. 22(a)-*marked with vertical double-headed arrow*). The difference is ∼3 meV. Secondly, from -4 nm to the vertex, the slope for the STS parameter containing edge (parallel case) has a comparatively greater slope (*marked with green arrow*). Thirdly, the parabolic-like trend in the vertex case has broader latus-rectum, i.e., wider horizontal spread of the curve or larger radius and smaller curvature (Fig. 22(a) - *marked with* **A** *and* **B**), **A**>**B**. The broadening of the onset energy in the vertex case is greater than the parallel case (Fig. 22(a)). As mentioned earlier, the edges affect the broadening and so the lifetime. A decrease of ∼12% in a lifetime is calculated for the electron in the presence of the edge. Further, the major change in the processes occurs at -4 nm from the vertex (*marked with green arrow*). And for the electron population, an inverted parabolic trend is seen near the vertex. At -4 nm,

both the curves tangentially pass each other (*marked with green arrow*). Afterward, a brief rise and followed-by a sharper drop are seen. Again, the vertex has shown a larger radius and smaller curvature than the parallel case. To conclude, the edge contributes towards a considerable change in LDOS even though the vertex has a pronounced effect.

4.8.2. LDOS on the Upper Terrace

The STS spectra recorded opposite to the polar edge [011] of the NaCl(100) on the upper terrace have resulted in a higher electron population. A similar result has been displayed by the STS spectrum in Sec. 4.6 - **L5** (Pg. 35). Apart from this topography, the electron population over the upper terrace is higher than the lower terrace in simple defects in the Ag(111) (**Section I**).

The Smoluchowski smoothing effect leads to a dipole at the step edges of the Ag(111). Later, the adsorbate preferably adsorbs at the step edges, exposing the respective ion to compensate for the step edge polarity. So, NaCl(100) forms a bilayer at the Ag(111) step edge (Fig. 23(b)) [15]. Hence, the Cl^- anion of the NaCl(100) is located on the top of the bilayer at the border of the step edge Fig. 23(a-i) [6]. The outcome is the NaCl(100) has a polar edge in $\langle 011 \rangle$ direction. Due to the anions collected at the top of the step edge, incoming electrons are back-scattered. This effect leads to a higher electron population on the upper terraces. On the hypothetical ground, anion creates a charge zone across the polar edge of the NaCl[011] that repels the incoming electron. A schematic view of the anion charge zone is presented in Fig. 23(b). Further, in Fig. 23(a-ii), the adsorption of the positive ion at the top edge of the step edge can not be omitted [6]. However, we limit our work to the earlier case of the anion adsorption to the top part of the step edges.

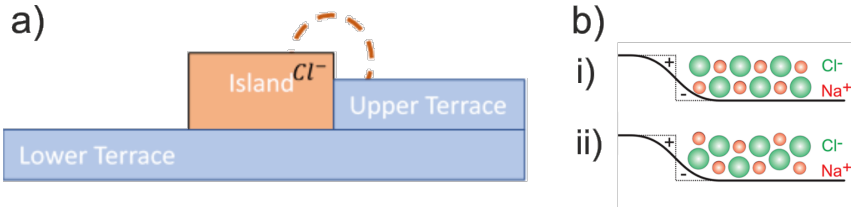

Figure 23: Schematic presentation of relative topography of a NaCl[011] polar edge adsorption. (a) A possible arrangement of the NaCl(100) adsorption to the step edge of the Ag(111) [6]. (b) Anion zone creation due to the polar edge [011] of the NaCl(100) at the step edges of the Ag(111).

This preference in NaCl arrangement at the step edges of the Ag(111) becomes apparent from the present STS measurement. A short comparison is done here to evaluate the

impact of the polar edge on the STS. The respective STS parameters are listed in Tab. 5. The values are measured at ∼6 nm from the slip plane dislocation and similar for the polar edge [011] of the NaCl(100). Since the furthest STS point existing from the polar edge is at ∼6 nm in Sec. 4.6 - **L5**, therefore this distance has been selected for creating uniformity. However, to exactly see the anion charge zone impact on the STS taken adjacent to it, refer STS spectrum - **L4** in Table 4 (Pg. 36). The electron population is comparatively low. So, this rationalizes the argument that the charge zone affects the electron population spatially.

Table 5: STS parameters of probing the upper terrace of Ag(111) and opposite to NaCl[011] edge.

STS Point	**E**/meV	△/meV	**I**/ arb. unit
Slip Plane Disl.	-66 ± 5	17 ± 4	226 ± 16
Sec. 4.6 - **L5**	-67 ± 2	12 ± 1	540 ± 77
Present Case	-66 ± 2	17 ± 4	315 ± 36

The electron population is the only parameter of the STS that has undergone considerable change compared to the onset energy and the broadening. This significant change can be attributed to the presence of the polar edge of the NaCl(100).

5. Conclusion and Outlook

In this thesis, a collective approach has been adopted to present the change in the electron behaviour, dynamics, and relative change in the population near 1-dimensional defects. The surface state electron adequately responds to the environment and differentiates among the defect, adatom, and adsorbate. Therefore, surface state electron can act as a probe [2]. Our work encompasses simple 1-dimensional defects in Ag(111) to a complex case of dielectric adsorbate NaCl(100) induced line-like defects on Ag(111) substrate.

Initially, the work encompasses simple 1-dimensional defect of the slip plane dislocation (Sec. 4.1 Pg. 18). The STS trends observed for the upper and the lower terrace then became the reference for the other cases in the thesis. Measurement of the LDOS is done spatially from the line dislocation. Further, the change in STS parameters, i.e., onset energy, broadening, and intensity, reflects the opening of the different scattering processes. The scattering processes involve electron-electron scattering (intraband transition) at the

bulk-surface mixing site, electron-phonon scattering (interband transition or phonon coupling), and electron-defect scattering. In addition, the Smoluochowski smoothing effect and lateral oscillation of the electron creating standing wave pattern affect the LDOS. The change in the onset energy over a distance of 8 nm towards the dislocation line is (12 ± 2) meV. The lifetime at the furthest STS recorded is (138 ± 28) fs. Whereas at the line dislocation is (323 ± 65) fs. Moreover, an ∼85% dropped in electron population at the slip plane dislocation. The second case investigated was the step edge defect. The factor that governed the LDOS was the presence of an atomic-scale roughness at the step edges (Sec. 4.2 Pg. 21). The STS parameter partially followed a similar trend to slip plane dislocation. The STS parameters evaluated here; the change in the onset energy over a maximum distance of 4 nm is (20 ± 3) meV, the broadening gives the lifetime to be (110 ± 15) fs at the furthest point and near the step edge defect is (233 ± 32) fs. The electron population has dropped to 80% from the furthest point to the defect site. So, the step edge defect has a more pronounced effect on the LDOS than the slip plane dislocation.

The investigated 2-dimensinonal defect constitutes a confined space for the surface electrons and point to additional surface states. The energy eigenstate is raised, which directly relates to the geometry of the confined space. The possible explanation is due to the conservation of mass. The change in onset energy is (14 ± 1) meV over a distance of ∼10 nm. The lifetime evaluated is (84 ± 17) fs and the electron population within the confinement has a lesser change in population towards the step edge defect (Fig. 16 Pg. 30).

In **Section II**, the STS investigates the different topography exhibited by the NaCl(100) island adsorbed on Ag(111). The LDOS was studied near a simple NaCl(100) island (Sec. 4.5 Pg. 32). The trends obtained for the STS parameters has shown similarity in trend but less in amplitude to the slip plane dislocation (Sec. 4.1, Pg. 18). The island has affected the LDOS up to ∼25 nm. The change in onset energy over a distance of 30 nm is (10 ± 1) meV. However, at the furthest point, the lifetime is (138 ± 28) fs and near the island (98 ± 12) fs. The lifetime is substantially dropped near the island. The electron population is roughly dropped three-fold (75%) near the island.

Next, the NaCl(100) adsorbed at the step edges of the Ag(111) exposing the polar edge-[011] of the triangular-shaped island. The adsorbate-substrate system becomes complicated from this point onwards. To understand the influence on the LDOS, the STS was recorded in different directions with respect to the island. These include STS (i) across the [001] edge (Sec. 4.6 Pg. 35), (ii) parallel to non-polar edge $[0\bar{1}0]$ (Sec. 4.7 Pg. 37), and (iii) $[0\bar{1}\bar{1}]$ bifurcating the NaCl(100) island (Sec. 4.8 Pg. 40) into mirror image. The STS

parameters evaluated in each part of the above-mentioned case result in a distinct set of values, solely attributed to the island topography and the STS recording direction. In (i) Sec. 4.6 (Pg. 35), the onset energy before and after the island roughly remains the same, i.e., (-63 ± 4) meV. The change occurred in the lifetime before the island, (134 ± 19) fs and after (150 ± 30) fs. Further, the electron population has increased after the island (on the upper terrace and opposite to the polar edge) by two-fold. In (ii) Sec. 4.7 (Pg. 37), four different regions were identified across the STS spectra. Two quantities changed considerably. Electron population and lifetime. There the vertex and non-polar edges affected the LDOS largely. The beginning of the STS spectra has lifetime = (61 ± 10) fs, near the vertex it becomes (76 ± 13) fs, adjacent to the non-polar edge $[0\bar{1}0]$ is (190 ± 30) fs, and at the junction (122 ± 25) fs (Fig. 20). The electron population is the highest opposite to the vertex in the 2 nm radius and least near the junction. And in (iii) Sec. 4.8 (Pg. 40), the STS was recorded across the island and bifurcated into a mirror image (Fig. 22). The lifetime near the vertex is (138 ± 18) fs and after the island on the upper terrace and opposite to the polar edge is (122 ± 25) fs. The electron population is increased 6% on the upper terrace compared to the vertex.

Out of these STS spectra, the following effects on electron LDOS are derived. (**a**) two-dimensional barrier exhibited by the step edge act as a confinement and ordained the electron to behave similar to the electron in the confinement, (**b**) the step edges of the NaCl(100) and Ag(111) act differently, this is indicated via the percentage change in the electron population. (**c**) The vertex and edge influence towards the electron LDOS differently. Vertex partly behaves as a point defect, which leads to localized perturbation in the proximity (Fig. 20-*small red circled marked* - ***a***). Whereas a step edge act as lateral confinement to the electron and leads to simple resonator [2]. Moreover, vertex offers the maximum electron population in a circular limit. (**d**) Lateral confinement of an electron in the proximity of the vertex and the salt edge results in the display of multiple peaks in x and y-direction. (**e**) The coarse structural setup of adsorbate and substrate leads to loss in dI/dV (Fig. 20-**Junction**). And finally, (**f**) the spectra recorded over the upper terrace and opposite to the polar edge of the NaCl[011], the electron population turns out relatively higher than the simple STS spectra recorded over the upper terrace. It signifies the presence of an anion charge zone that repels the electron.

Outlook:

Getting a defined structured barrier has prompted the nanotechnological world to exploit the fabrication and manufacturing arena to the next level. Artificially adatom-like Fe becomes the scattering center [16] and porphyrin molecules behave to form confinement

for a smaller molecule [?]. Further, macrocycles create opportunities to carry out the reaction within the confined environment of the macro-molecules [?].

Here, I forward three suggestions that can help communities link with the STM and the Nanoengineering.

(**I**) **Vertx-Confinement System**: Since the vertex of the salt offered localized perturbation and relatively high electron population. Designing the dielectric adsorbate into the confined space (Fig. 24(a)) will help in maneuvering and transforming the localized perturbation into quantized energy states.

(**II**) **QuadGon**: The second outlook of the work is the engagement of the quantum confinement or particle-in-a-box physics. A quadrilateral (4 sided polygon) with the opposite sides facing each other have a dielectric adsorbate (like NaCl(100)) and the other two opposites sides with a metallic substrate (Fig. 24(b)). Since in one of our cases, LDOS was affected in the presence of the step edge of the Ag(111) near the NaCl(100) island (Sec. 4.6 Pg. 35). This model can become a part of a commercial enterprise.

(**III**) **BOOLEAN GATE**: The third and last one is building a cascading system on the substrate. This is probably achievable by structurally setting up a sandwich-like structure between salt and substrate (Fig. 24(c)). This can facilitate the AND/OR gate possibilities via electron-rich to electron-poor physically viable states.

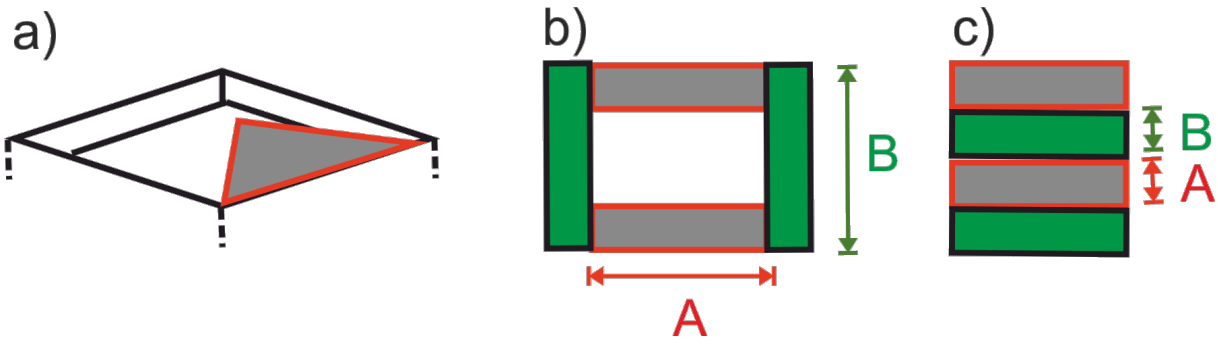

Figure 24: Schematic presentation of possible structures for future research. Here gray colour represents salt and green colour represents metallic substrate. **A** and **B** means the width or length of the respective entity. (a) A salt island within a confined space. (b) QuadGon or Quadrilateral Polygon leads to quantum well effect. And (c) BOOLEAN Gate. A sandwich-like structure is constructed on the substrate.

These suggested systems are hard to fabricate, but the science within them will help in

deciphering phenomena that are uncommon and non-trivial, i.e., quantum phenomena, magnetic properties, and spin-exhausted systems.

A. Appendix: Step Edge Defect - *dI/dV*

Following raw data is presented which has been considered for the preparation of the results. Each figure contains *dI/dV* of the STS datapoints. Total of 10 datapoints were recorded across the step edge defect. For an STM figure, refer Fig. 12 (Pg. 22).

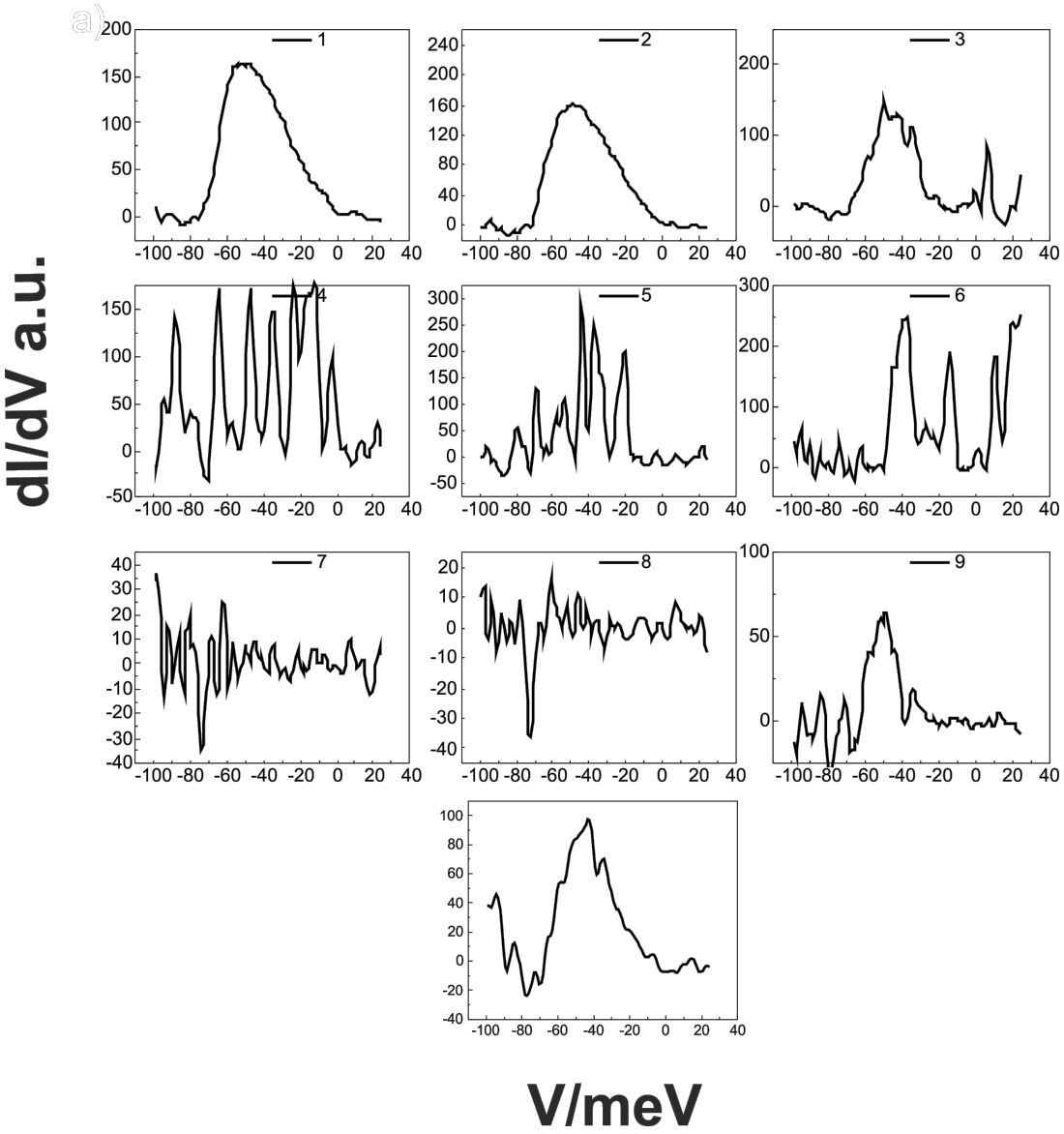

Figure 25: Set-i *dI/dV* of the step edge defect. Each window is marked with the respective STS datapoint.

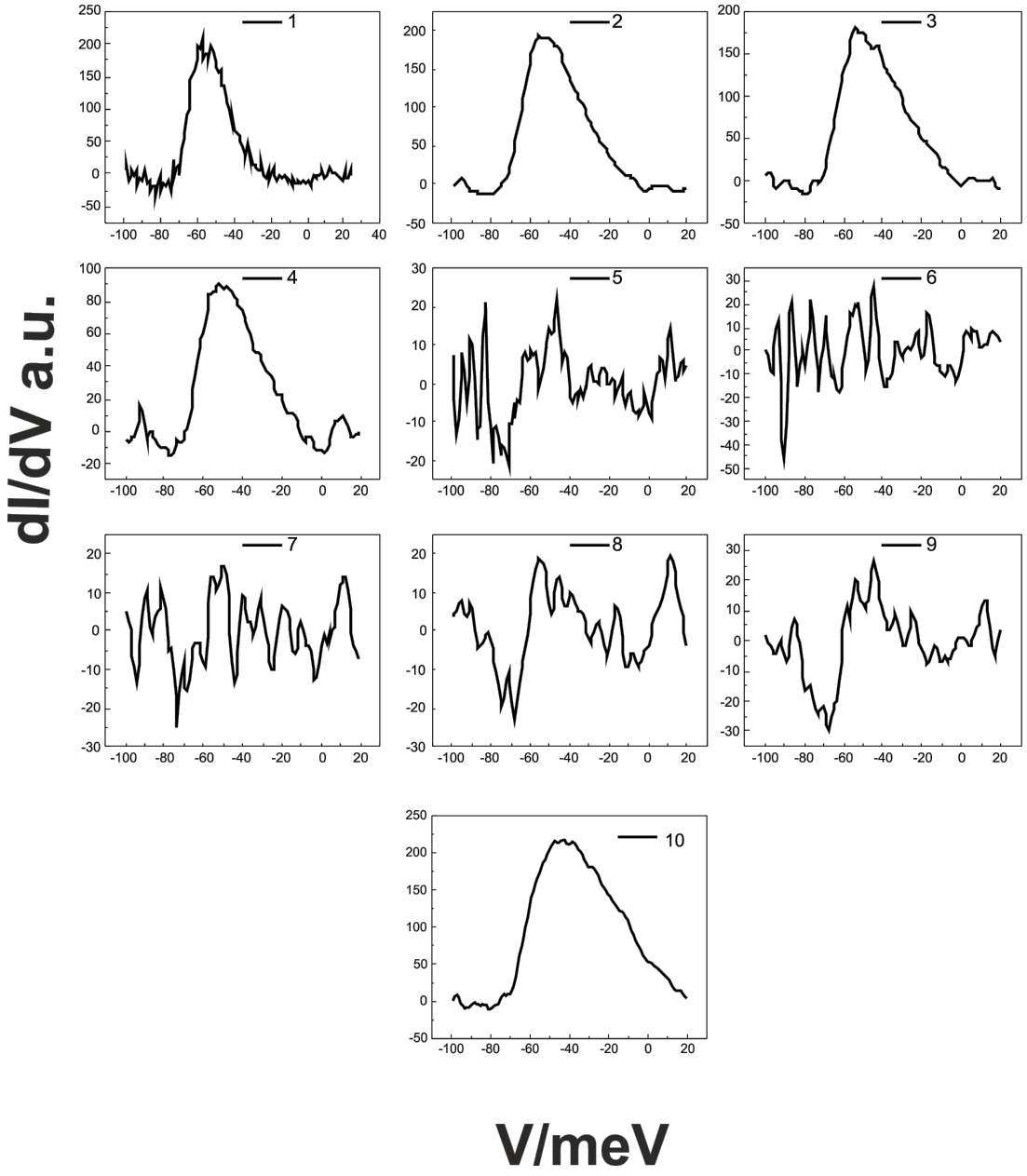

Figure 26: Set-ii dI/dV of the step edge defect. Each window is marked with the respective STS datapoint.

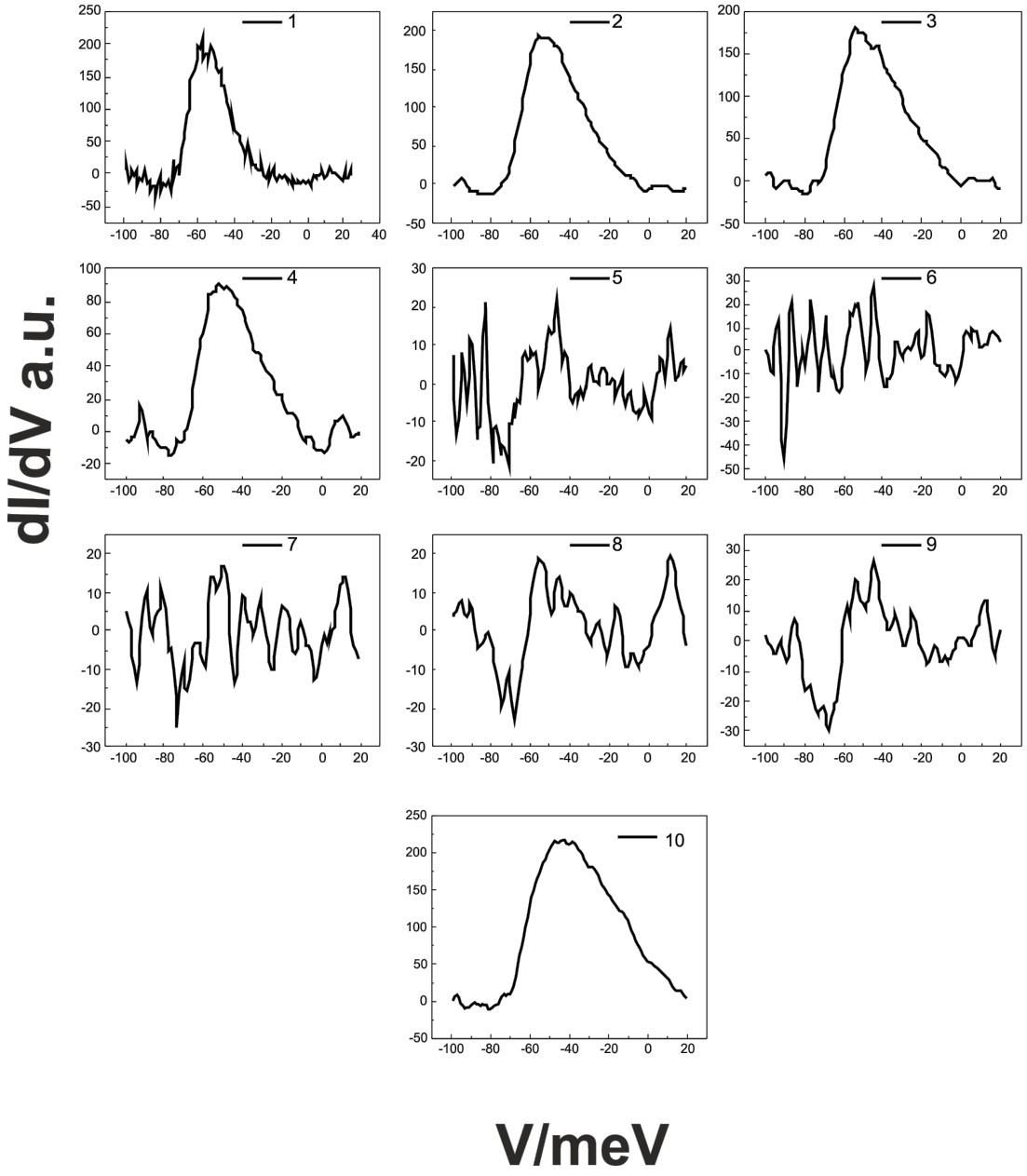

Figure 27: Set-iii dI/dV of the step edge defect. Each window is marked with the respective STS datapoint.

Acknowledgement

I would like to express my deep gratitude to Prof. Dr. Karina Morgenstern for accepting me into her group to carry out the research work. Her enthusiastic encouragement towards my research ideas and useful critiques has bestowed me with a deeper understanding of Surface Science. I am also thankful to Dr. Niklas Osterloh for continuous help and timely suggestions on the matter related to STM and research work. And in the end, I am thankful to each member of the group for their untiring support over this period.
Further, I am thankful to IMOS faculty and staff for their trust and support in conducting my research studies and for all the resources granted to us during the meantime.

References

[1] P.M. Echenique, R. Berndt, E.V. Chulkov, Th. Fauster, A. Goldmann, and U. Höfer. Decay of electronic excitations at metal surfaces. Surface Science Reports, 52(7-8):219–317, may 2004.

[2] Karina Morgenstern, Nicolas Lorente, and Karl-Heinz Rieder. Controlled manipulation of single atoms and small molecules using the scanning tunnelling microscope. physica status solidi (b), 250(9):1671–1751, jul 2013.

[3] K W Hipps. Handbook of Applied Solid State Spectroscopy. Springer-Verlag GmbH, July 2006.

[4] Richard Berndt O. R. Bryant S. Crampin Jiutao Li, Wolf-Dieter Schneider. Surface-state lifetime measured by scanning tunneling spectroscopy. Physical Review Letters (1998) 81(20) 4464-4467, 1998.

[5] K. Oura, M. Katayama, A. V. Zotov, V. G. Lifshits, and A. A. Saranin. Surface Science. Springer Berlin Heidelberg, 2003.

[6] S. Heidorn, B. Gerss, and K. Morgenstern. Step edge induced reconstructions of nacl(100) bilayers on ag(111): A route to alter the properties of nanoscale insulators. ACS Applied Nano Materials, 1(12):6818–6823, 2018.

[7] Karina Morgenstern, Kai-Felix Braun, and Karl-Heinz Rieder. Surface-state depopulation on small ag(111) terraces. Physical Review Letters, 89(22):226801, nov 2002.

[8] V. G. Lifshits, Alexander A. Saranin, A. V. Zotov, M. Katayama, and K. Oura. Surface Science. Springer-Verlag GmbH, May 2003.

[9] Lutz-C. Eigler D. Crommie, M. Imaging standing waves in a two-dimensional electron gas. Nature 363, 524–527, 10 June 1993.

[10] Julian Koch. Untersuchung der energie und derlebensdauer des grenzachenzustandszwischen nacl(100) und ag(111), 2012.

[11] Freie Universität Berlin Repository, editor. The experimental and theoretical techniques: an introduction. Freie Universität Berlin Repository.

[12] Flemming Besenbacher Karina Morgenstern, Erik Laegsgaard. Quantum size effects in adatom island decay. Physical Review Letter, 2005 Apr 29.

[13] Friederike Matthaei, Sarah Heidorn, Konrad Boom, Cord Bertram, Ali Safiei, Jörg Henzl, and Karina Morgenstern. Coulomb attraction during the carpet growth mode of NaCl. Journal of Physics: Condensed Matter, 24(35):354006, aug 2012.

[14] Sarah Heidorn and Karina Morgenstern. Spatial variation of the surface state onset close to three types of surface steps on ag(111) studied by scanning tunnelling spectroscopy. New Journal of Physics, 13(3):033034, mar 2011.

[15] Sarah-Charlotta Heidorn, André Sabellek, and Karina Morgenstern. Size dependence of the dispersion relation for the interface state between NaCl(100) and ag(111). Nano Letters, 14(1):13–17, dec 2013.

[16] M.F. Crommie, C.P. Lutz, D.M. Eigler, and E.J. Heller. Quantum corrals. Physica D: Nonlinear Phenomena, 83(1):98–108, 1995. Quantum Complexity in Mesoscopic Systems.

[17] J. Kliewer. Dimensionality effects in the lifetime of surface states. Science, 288(5470):1399–1402, may 2000.

[18] D. J. Bacon Derek Hull. Introduction to Dislocations. Elsevier Science Techn., July 2001.

[19] S. Heidorn, C. Bertram, J. Koch, K. Boom, F. Matthaei, A. Safiei, J. Henzl, and K. Morgenstern. Influence of substrate surface-induced defects on the interface state between nacl(100) and ag(111). Journal of Physical Chemistry C, 117:16095–16103, 2013.

[20] Ph. Avouris, I.-W. Lyo, and P. Molinàs-Mata. Stm studies of the interaction of surface state electrons on metals with steps and adsorbates. Chemical Physics Letters, 240(5):423–428, 1995.